Jℳ PAPERS

Optimising branched fluidic networks: a unifying approach including laminar and turbulent flows, rough walls and non-Newtonian fluids

J.S. Smink[1] , **R. Hagmeijer**[1] , **C.H. Venner**[1] **and C.W. Visser**[1]

[1]Engineering Fluid Dynamics group, Faculty of Engineering Technology, University of Twente, Enschede, the Netherlands

Corresponding author: J.S. Smink, j.s.smink@utwente.nl

Power minimisation in branched fluidic networks has gained significant attention in biology and engineering. The optimal network is defined by channel radii that minimise the sum of viscous dissipation and the volumetric energetic cost of the fluid. For limit cases including laminar flows, high-Reynolds-number turbulence or smooth-channel approximations, optimal solutions are known. However, current methods do not allow optimisation for a large intermediate part of the parameter space which is typically encountered in realistic fluidic networks that exhibit turbulent flow. Here, we present a unifying optimisation approach based on the Darcy friction factor, which has been determined for a wide range of flow regimes and fluid models and is applicable to the entire parameter space: (i) laminar and turbulent flows, including networks that exhibit both flow types, (ii) non-Newtonian fluids (powerlaw, Bingham and Herschel–Bulkley) and (iii) networks with arbitrary wall roughness, including non-uniform relative roughness. The optimal channel radii are presented analytically and graphically. All existing limit cases are recovered, and a concise framework is presented for systematic optimisation of fluidic networks. Finally, the parameter x in the optimisation relationship $Q \propto R^x$, with Q the flow rate and R the channel radius, was approximated as a function of the Reynolds number, revealing in which case the entire network can be optimised based on one optimal channel radius, and in which case all radii must be optimised individually. Our approach can be extended to a wide range of fluidic networks for which the friction factor is known, such as different channel curvatures, bubbly flows or specific wall slip conditions.

Key words: fractals, channel flow, rheology

J.S. Smink, R. Hagmeijer, C.H. Venner and C.W. Visser

1. Introduction

Branched networks for fluid transport are omnipresent in biology and engineering. Biological systems, such as vascular networks (Hutchins, Miner & Boitnott 1976; Reichold *et al.* 2009; Kelch *et al.* 2015) and the bronchial trees of the lungs (Hooper 1977; Xu *et al.* 2016; Sznitman 2022), are capable of efficiently transporting heat or mass with low dissipation within limited volumes (Bejan & Lorente 2013). Similarly, fluidic networks provide efficient transport in emerging engineering applications, such as microfluidics (Whitesides 2006), additive manufacturing (Skylar-Scott *et al.* 2019; Shaqfeh *et al.* 2023), creation of synthetic vasculatures (Sexton *et al.* 2023), microreactors (Dong *et al.* 2021) and multifunctional materials (Zheng *et al.* 2017). These networks were comprehensively analysed and optimised for Newtonian (Murray 1926*a*,*b*; Kamiya, Togawa & Yamamota 1974; Zamir 1977; Oka & Nakai 1987), power-law (Mayrovitz 1987; Revellin *et al.* 2009; Stephenson & Lockerby 2016; Miguel 2018) and yield-stress fluids (Ponalagusamy 2012; Smink *et al.* 2023) in the laminar flow regime. However, a transition to turbulence commonly occurs in natural flows (Olson, Dart & Filley 1970; Stein & Sabbah 1976; Ku 1997; Berger & Jou 2000; Calmet *et al.* 2016; Ha *et al.* 2018, 2019) and industrial flows such as district heating (Gumpert, Wieland & Spliethoff 2019; Steinegger *et al.* 2023), water distribution networks, heat exchangers (Siddiqui & Zubair 2017), the paper making process (Lundell, Söderberg & Alfredsson 2011) and inertial microfluidics (Wang, Yang & Zhao 2014). Similarly, fluidic networks that exhibit both turbulent flow and non-Newtonian behaviour may benefit upscaling of nozzle-based technologies via parallelisation, such as in-air microfluidics (Visser *et al.* 2018), spray drying (van Deventer, Houben & Koldeweij 2013), prilling (Kamis *et al.* 2023) or 3D printing of polymer foams (Visser *et al.* 2019). Finally, analytical optimisation of fluidic networks in various turbulent regimes would provide key validation data for computational fluid dynamics, which is increasingly used to describe (Morris *et al.* 2016) or design (Sexton *et al.* 2023) networks with e.g. complex geometries.

The parameter space spanned by the Reynolds number, the roughness and different fluid models is shown in figure 1(*a,b*). Applications are plotted in figure 1(*a*), showing the broad range of relevant Reynolds numbers, *Re*, and relative channel wall roughnesses, δ, especially in the intermediate-*Re* turbulent regime (the Reynolds number is defined in (2.4)). Figure 1(*b*) shows that the energy consumption by the network has been minimised (Murray 1926*b*; Smink *et al.* 2023) only for specific limits of this parameter space. This total energy consists of the sum of the power needed to maintain the flow (product of the pressure drop Δp and the volume flow rate Q) and a volumetric cost function αV, with α a cost factor and V the volume of the channel, for networks as schematically shown in figure 1(*c, d*). For example, in the case of a vascular network, the cost factor expresses the metabolic energy needed to maintain blood ($\alpha \approx 1\,\mathrm{kW\,m^{-3}}$) (Murray 1926*b*); for other situations, see Smink *et al.* (2023). Note that optimising the relative channel radii for a given volume is a related problem, which has been pursued for many cases with e.g. a constructional law (Bejan, Rocha L.A. & Lorente 2000; Miguel & Rocha 2018; Miguel 2018). Instead, we focus on optimisation against a cost factor, which is generalisable for different boundary conditions such as a cost function of the wall surface area (Woldenberg & Horsfield 1986) and readily provides access to the optimal channel radii.

For a circular pipe with radius R, the power is generally minimised if
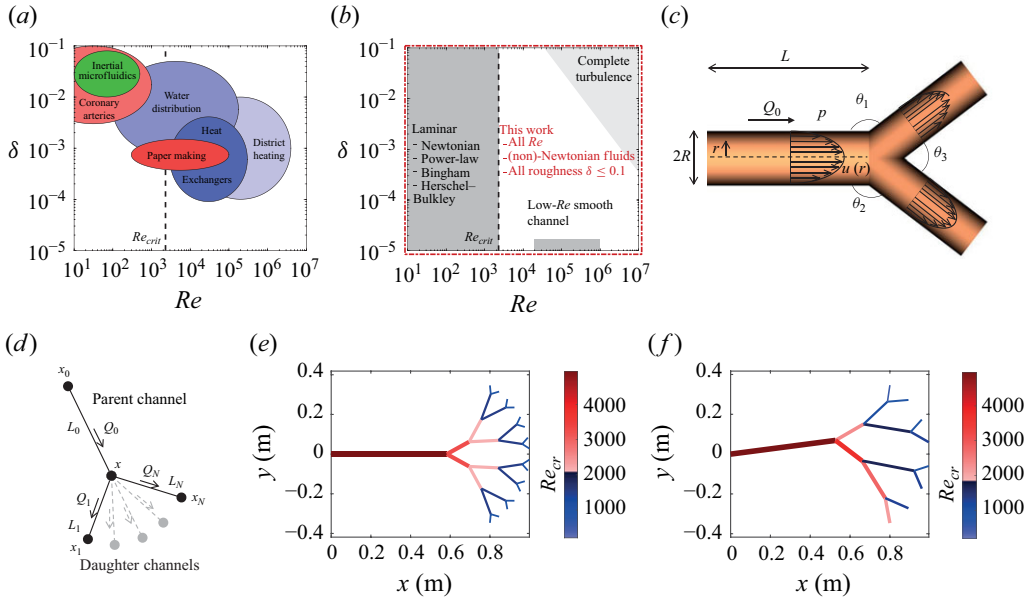
$$\frac{R^x}{Q} = \mathrm{const.}, \tag{1.1}$$

Figure 1. (*a*) Parameter space of the Reynolds number *Re* and the relative channel wall roughness δ for fluidic networks in coronary arteries (Singhal, Henderson & Horsfield 1973; Kassab *et al.* 1993; Burton & Espino 2019), paper making (Forgacs, Robertson & Mason 1957; Grossman & Carpenter 1968; Moller 1976), water distribution (van der Schans *et al.* 2015; NEN 2018), inertial microfluidics (Di Carlo 2009; Zhang *et al.* 2016; Lu *et al.* 2017), heat exchangers (Towler & Sinnott 2013) and district heating (Gumpert *et al.* 2019; Steinegger *et al.* 2023). The colour indicates a Newtonian (blue), power-law (green) or yield-stress (red) fluid. Here, Re_{crit} is assumed to be independent of δ for this parameter space. (*b*) Previously optimised parts of the parameter space include laminar flow and low-*Re* turbulent flow in a smooth channel and a specific condition for complete rough-channel turbulence. (*c*) Schematic of a single branch with fully developed laminar flow profiles within the channels. (*d*) Schematic of a branched fluidic network, where a parent channel splits up into *N* daughter channels. The location of the branching point $\boldsymbol{x}$ follows from the analysis and determines the lengths L_i of the channels. The grey channels indicate that it is possible to have many channels that originate from the branching point. (*e*, *f*) Examples of optimised branched fluidic networks. The colour indicates the Reynolds numbers in the channel. The position coordinates of the begin and endnodes are given as an input; the coordinates of intermediate nodes follows from the optimisation. Also the flow rates in all channels are given as an input. The following quantities are kept constant: $Q_0 = 20$ l min^{-1}, $\rho = 1000$ kg m^{-3}, $\alpha = 10^3$ W m^{-3} and $\tau_0 = 0$ Pa. Fluid and system parameters are defined in § 2. (*e*) Newtonian fluid in rough channel ($\mu' = 10^{-3}$ Pa s, $n = 1.0$, $\varepsilon = 10^{-5}$ m, 5 levels, symmetric branching). (*f*) Power-law fluid in smooth channel ($\mu' = 5 \times 10^{-5}$ Pa s$^{1.5}$, $n = 1.5$, 4 levels, asymmetric branching 1:2).

with *x* a flow-regime and fluid-model-dependent power; $x = 3$ for laminar flow of an incompressible Newtonian fluid, as further analysed theoretically (e.g. revealing the shear forces, the optimal angles between channels or special cases such as curved pipes or porous channels) (Kamiya *et al.* 1974; Zamir 1977; Sherman 1981; Miguel 2018) and verified experimentally for e.g. human coronary and cerebral arteries (Hutchins *et al.* 1976; Rossitti & Löfgren 1993). The value $x = 3$ also holds for laminar flows of different fluid models, including power-law (Mayrovitz 1987; Revellin *et al.* 2009; Stephenson & Lockerby 2016; Miguel 2018) and yield-stress fluids, such as the Bingham, Herschel–Hulkley and Casson models (Smink *et al.* 2023), as well as for channels with elliptical (Tesch 2010) and rectangular (Emerson & Barber 2012), or even arbitrary cross-sections (Emerson *et al.* 2006; Stephenson *et al.* 2015; Zhou *et al.* 2024).

For turbulent flows, fluidic networks were optimised only for limit cases and approximations (Uylings 1977; Woldenberg & Horsfield 1986; Bejan *et al.* 2000;

Stephenson & Lockerby 2016). For turbulent flow of Newtonian fluids at intermediate Reynolds numbers $2 \times 10^4 < Re < 10^6$ in a hydraulically smooth channel (shaded for relative wall roughness $\delta \to 0$ in figure 1*b*), $x = 17/7$ was derived from an empirical relation for the friction factor (Bejan 2013; Kou *et al.* 2014). For complete turbulence (the light-shaded area in figure 1(*b*), which is defined as $Re > 3500/\delta$ Moody 1944), it was derived that $x = 7/3$ (Uylings 1977; Bejan *et al.* 2000; Williams *et al.* 2008; Stephenson & Lockerby 2016). Several previous studies (e.g. Revellin *et al.* 2009 and Zhou *et al.* 2024) have generalised the optimisation procedure for friction factors that are a power-law function of R, and show that all these limit cases can be described by a single approach. However, the intermediate part of the parameter space is described by more complex friction factors that cannot be implemented in these existing approaches, such as the Colebrook–White equation. Stephenson *et al.* (2015) and Stephenson & Lockerby (2016) use a different approach allowing friction factors in arbitrary functional form, but they do not apply this to the intermediate part of the parameter space. This *terra incognita* represents a major knowledge gap, both fundamentally, as it covers several orders of magnitude of both Re and δ, and from an application perspective, as we will show that turbulent limit cases are rarely reached for realistic flows.

In this study, we introduce a universal approach for optimising fluidic networks in the entire parameter space. The optimisation procedure is applicable to any flow regime, wall roughness or fluid model for which the Darcy friction factor is known, even if its formulation is implicit. First, § 2 describes non-dimensionalisation of pipe flows, enabling calculation of the optimal Reynolds number within a channel and the corresponding channel radius. Subsequently, the optimal channel radius is derived for laminar and turbulent flow at arbitrary Re, arbitrary channel roughness δ and for both Newtonian and non-Newtonian fluids in § 3. Section 4 synthesises the results from §§ 2 and 3, resulting in approximations of x as a function of Re for all flow regimes and fluid models. The design procedure is presented in § 5. The conclusions are presented in § 6. The design of the optimal location of branching points within the network is described in Appendix A.1, resulting in fully optimised networks for e.g. rough-wall channels (figure 1*e*) or for non-Newtonian fluids (figure 1*f*). Finally, an application example is provided in Appendix F.

2. Optimisation of fluidic branching

Consider a branching configuration comprising a parent channel connected to N daughter channels at a branching point denoted as $\boldsymbol{x}$, as depicted in figure 1(*d*). The channels are labelled 0 to N, with index 0 indicating the parent channel. The effective radii of the channels are represented as $\boldsymbol{R} \equiv (R_0, R_1, \ldots, R_N)$, while the termination points of the channels are fixed and denoted as $\boldsymbol{x}_i$ for $i = 0, 1, \ldots, N$. The flow rates in the daughter channels are specified as Q_i for $i = 1, \ldots, N$, with Q_0 corresponding to the flow rate in the parent channel; Q_0 is considered positive towards the branching point, whereas the flow rates in the daughter channels (Q_i, $i = 1, \ldots, N$) are taken positive away from the branching point. To ensure mass conservation, assuming incompressibility, the flow rates must satisfy $Q_0 = \sum_{i=1}^{N} Q_i$. The lengths of the channels, L_i, are functions of the branching location, given by $L_i \equiv |\boldsymbol{x}_i - \boldsymbol{x}|$ for $i = 0, 1, \ldots, N$. In this work, it is assumed that there is only an axial velocity u. The channels are assumed to be cylindrical with $R \ll L$. The fluid properties are taken constant and the flow is fully developed.

For optimisation of a fluidic network, the power to maintain the flow and to maintain a fluid is minimised. The power is represented by a cost function depending on the radii and

lengths of the channels, and is the sum of the individual channel contributions

$$P(\boldsymbol{R}, \boldsymbol{x}) \equiv \sum_{i=0}^{N} (\Delta p_i \, Q_i + \alpha V_i). \qquad (2.1)$$

Here, $V_i \equiv \pi R_i^2 L_i$ is the channel volume and the pressure gradient $\Delta p/L$ is a fluid-type and flow-regime-dependent function. The pressure at the nodes is not defined or constrained. Differentiation of (2.1) to $\boldsymbol{R}$ and $\boldsymbol{x}$ and equating these expressions to 0 provides the optimisation problems for: (i) the channel radii $\boldsymbol{R}$, and (ii) the location of the branching point $\boldsymbol{x}$ (optimised in Appendix A.1). Optimisation of the channel radius is independent of $\boldsymbol{x}$, because it is a decoupled problem (Smink *et al.* 2023), in which the power defined by (2.1) attains a global minimum with respect to the radius if all channels satisfy $\partial P/\partial \boldsymbol{R} = \boldsymbol{0}$. Therefore, the optimisation condition for any radius R_i only depends on the power contribution of the corresponding channel and R_i does not depend on the lengths of the channels L_i.

For minimising the power consumption in the network, every single channel has to be optimised individually according to

$$\frac{\partial P}{\partial R_i} = \frac{\partial \Delta p_i}{\partial R_i} Q_i + 2\pi \alpha R_i L_i = 0, \quad i = 0, 1, \dots, N. \qquad (2.2)$$

The pressure drop Δp is represented as a function of a flow rate Q and a radius R using the Darcy–Weisbach equation (Weisbach 1845)

$$\Delta p = f \frac{\rho}{4\pi^2} \frac{Q^2}{R^5} L. \qquad (2.3)$$

Here, ρ is the fluid density, L is the length of the channel and f the Darcy friction factor. The friction factor f as function of the Reynolds number for the different fluid models is presented in figures 2(*b*)–2(*d*). The specific equations of f for different flow regimes and fluid models are provided in § 3. In this study, a generalised Reynolds number is defined as (Garcia & Steffe 1986)

$$Re \equiv \frac{8}{\pi^{2-n}} \left(\frac{n}{3n+1} \right)^n \frac{\rho}{\mu'} \frac{Q^{2-n}}{R^{4-3n}}. \qquad (2.4)$$

The value of f also depends on the Hedström number He (commonly used for description of yield-stress fluids), the relative wall roughness $\delta \equiv \varepsilon/2R$ (where ε is the absolute channel wall roughness) and the flow index n.

The effective dynamic viscosity μ describes the resistance of a fluid against shear, and is defined as $\mu = \mu'|\dot{\gamma}|^{n-1}$, where $\dot{\gamma}$ is the shear rate, μ' is the flow consistency index and n the flow index, where $0 < n < 1$ represents a shear-thinning and $n > 1$ represents a shear-thickening fluid, as shown in figure 2(*a*). In addition, a fluid may show yield-stress behaviour if $\tau_0 \geqslant 0$ (e.g. Bingham and Herschel–Bulkley fluids, see figure 2*a*), where the fluid only shears once an effective local shear stress exceeds the yield stress τ_0. The rheological behaviour for the shear rate of a Herschel–Bulkley fluid as function of the effective local shear stress is described as

$$\dot{\gamma}(\tau) = \begin{cases} \text{sign}(\tau_{rz}) \left(\frac{|\tau_{rz}| - \tau_0}{\mu'} \right)^{1/n} & \text{if } |\tau_{rz}| \geqslant \tau_0, \\ 0 & \text{if } |\tau_{rz}| < \tau_0, \end{cases} \qquad (2.5)$$
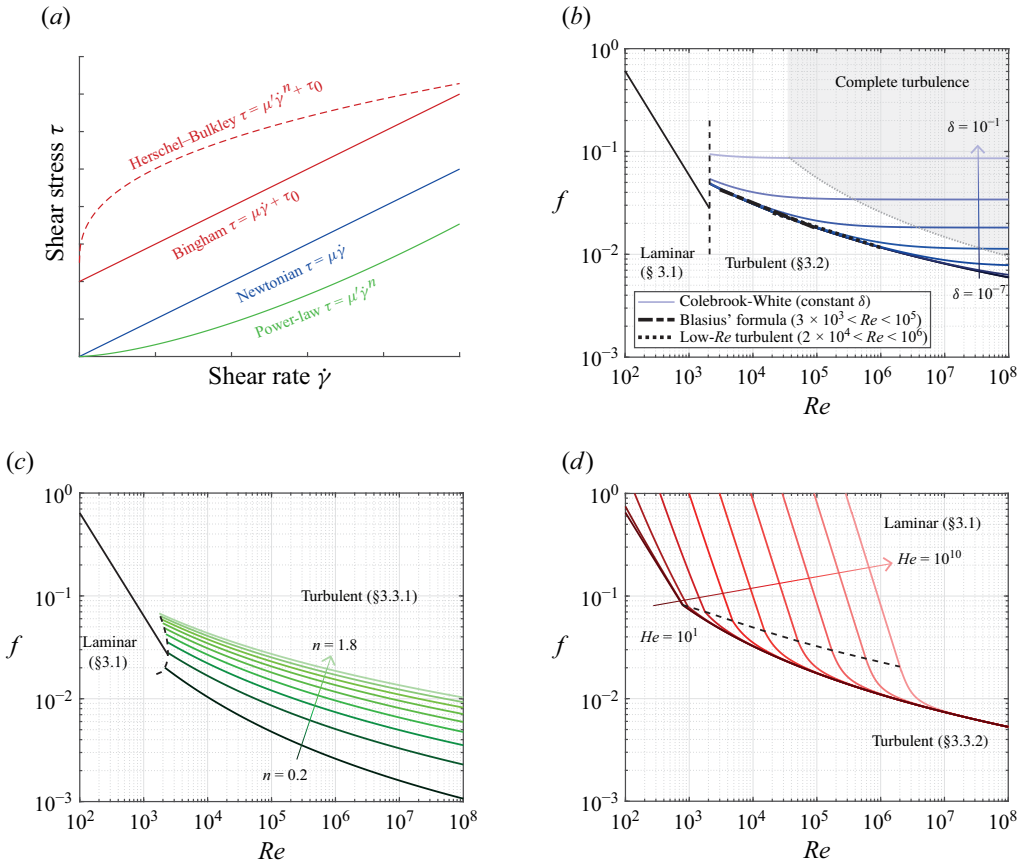
Figure 2. (*a*) Fluid models as analysed in this work. (*b–d*) Friction factor as function of the Reynolds number for different fluid models. The dashed black line indicates the transition from laminar to turbulent flow. (*b*) Newtonian fluid in rough channels (Moody diagram (Moody 1944)). The blue lines represent constant relative roughness δ from $10^{-7}, 10^{-6}, \ldots 10^{-1}$. (*c*) Power-law fluid in smooth channels. The green-scale lines represent values of the flow index n from $0.2, 0.4, \ldots 1.8$. (*d*) Herschel–Bulkley fluid with $n = 1.0$ in smooth channels. the red-scale lines represent constant values of the Hedström number from $10^1, 10^2, \ldots, 10^{10}$.

where τ_{rz} is the local shear stress induced by the flow. Figures 2(*b*)–2(*d*) also show the transition from laminar to turbulent flows at the critical Reynolds number (Hanks & Ricks 1974)

$$Re_{crit} = \frac{6464n}{(1+3n)^2} \times (2+n)^{(2+n)/(1+n)} \times \frac{\psi^{2-n}}{(1-\phi)^{(n+2)/n}}, \qquad (2.6)$$

where $\psi(\phi, n)$ and ϕ are defined in § 3.1. Although an increased relative roughness results in a decrease in Re_{crit}, this effect becomes only dominant around $\delta = 0.1$ and larger (Everts, Robbertse & Spitholt 2022). In order to ensure the validity of the used equations, the present study will limit the discussed optimisation results to $\delta \leqslant 0.1$.

The optimisation condition for the radius of every channel is obtained by substituting (2.3) into (2.2), providing

$$R^7 = \frac{\rho Q^3}{8\pi^3 \alpha} B, \qquad (2.7)$$

where B is defined as

$$B \equiv 5f - R\frac{\partial f}{\partial R}. \tag{2.8}$$

Here, B is a function of f and R and thus indirectly also a function of Re, He, δ and n.

The goal is to obtain an expression for the optimal channel radius as a function of parameters that are independent of R. Therefore, dimensional analysis is carried out to find a dimensionless form of the channel radius as function of radius-independent dimensionless groups (for more details, see Appendix A.2). Scaling of the optimisation problem results in the following 5 dimensionless numbers:

$$\tilde{R} \equiv \frac{R}{\rho^{-\frac{1}{2}}\mu'^{\frac{3}{2(n+1)}}\alpha^{\frac{n-2}{2(n+1)}}}, \quad \tilde{Q} \equiv \frac{Q}{\rho^{-\frac{3}{2}}\mu'^{\frac{7}{2(n+1)}}\alpha^{\frac{3n-4}{2(n+1)}}}, \quad \tilde{\tau}_0 \equiv \frac{\tau_0}{\mu'^{\frac{1}{n+1}}\alpha^{\frac{n}{n+1}}},$$

$$\tilde{\varepsilon} \equiv \frac{\varepsilon}{\rho^{-\frac{1}{2}}\mu'^{\frac{3}{2(n+1)}}\alpha^{\frac{n-2}{2(n+1)}}} \text{ and } n. \tag{2.9}$$

To align with the literature, the Reynolds number will be used instead of $\tilde{R}$. This choice will simplify the later computations in § 3 and enables direct characterisation of the flow in the channel. The Reynolds number is rewritten in dimensionless groups as follows:

$$Re = a(n)\frac{\tilde{Q}^{2-n}}{\tilde{R}^{4-3n}}, \tag{2.10}$$

where $a(n)$ is defined as

$$a(n) \equiv \frac{8}{\pi^{2-n}}\left(\frac{n}{3n+1}\right)^n. \tag{2.11}$$

The network is described by the dimensionless numbers Re, $\tilde{Q}$, $\tilde{\tau}_0$, $\tilde{\varepsilon}$ and n. As $\tilde{\tau}_0$, $\tilde{\varepsilon}$ and n are fluid or system parameters that are constant in a network, Re and $\tilde{Q}$ are the only flow-rate-dependent dimensionless numbers, which is convenient for network optimisation. Described with the new dimensionless numbers, f will now be a function of 5 dimensionless numbers instead of 4. Therefore, in the new domain, there will be a curve along which f is constant, removing one degree of freedom (see Appendix A.3).

For given fluid, flow and system properties, an optimal channel radius can be calculated via the Reynolds number using the non-dimensionalised optimisation condition (2.7)

$$(8\pi^3)^{4-3n}a^7\tilde{Q}^{2(n+1)} = \tilde{B}^{4-3n}Re^7, \tag{2.12}$$

where $\tilde{B}$ is a function of $\tilde{f}$, which is a function of Re, $\tilde{\tau}_0$, $\tilde{Q}$, $\tilde{\varepsilon}$ and n. Hence, (2.8) can be rewritten as

$$\tilde{B} = 5\tilde{f} - R\frac{\partial \tilde{f}}{\partial R} = 5\tilde{f} - R\frac{\partial \tilde{f}}{\partial Re}\frac{\partial Re}{\partial R} = \tilde{f}\left(5 + (4-3n)\frac{Re}{\tilde{f}}\frac{\partial \tilde{f}}{\partial Re}\right), \tag{2.13}$$

where differentiation of (2.4) provides $\partial Re/\partial R = -(4-3n)Re/R$. Therefore, knowing $\tilde{\tau}_0$, $\tilde{Q}$, $\tilde{\varepsilon}$ and n, one can determine the optimal Re for a channel.

We conclude this section by introducing dimensionless groups that will be used in § 3. The Hedström number He is defined (Swamee & Aggarwal 2011) and rewritten as follows:

$$He \equiv \frac{4R^2\rho}{\mu'}\left(\frac{\tau_0}{\mu'}\right)^{\frac{2-n}{n}} = 4\left(a(n)\frac{\tilde{Q}^{2-n}}{Re}\right)^{\frac{2}{4-3n}}\tilde{\tau}_0^{\frac{2-n}{n}}. \tag{2.14}$$

The relative roughness δ becomes in the new dimensionless groups

$$\delta \equiv \frac{\varepsilon}{2R} = \frac{1}{2}\,\tilde{\varepsilon}\left(\frac{Re}{a(n)\,\tilde{Q}^{2-n}}\right)^{\frac{1}{4-3n}}. \tag{2.15}$$

Characteristic for a yield-stress fluid is the formation of a plug in the centre of the channel, where the local shear stress τ_{rz} does not exceed the yield stress τ_0. The associated plug radius R_p is characterised by

$$R_p \equiv \frac{2\tau_0}{\dfrac{\Delta p}{L}}. \tag{2.16}$$

Non-dimensionalisation of the plug radius yields the dimensionless plug radius ϕ, which often appears in descriptions for f in the case of yield-stress fluids

$$\phi \equiv \frac{R_p}{R} = \frac{2\tau_0}{\dfrac{\Delta p}{L}R}. \tag{2.17}$$

By definition, ϕ can also be expressed in terms of the Reynolds and Hedström number and in the new dimensionless groups

$$\phi = \frac{64}{f\,Re}\left(\frac{2He}{Re}\left(\frac{n}{3n+1}\right)^2\right)^{\frac{n}{2-n}} = 8\pi^2 a(n)^{\frac{4}{4-3n}}\frac{\tilde{\tau}_0}{\tilde{f}\,Re}\left(\frac{\tilde{Q}^2}{Re^3}\right)^{\frac{n}{4-3n}}. \tag{2.18}$$

Up to here, no assumptions are made with respect to the flow type.

3. Network optimisation for different flow regimes and fluid models

The following flow regimes and fluid models are discussed in subsections:

- § 3.1 Laminar flow of a Newtonian and non-Newtonian fluids.
- § 3.2 Turbulent flow of Newtonian fluids, rough and smooth channels.
- § 3.3 Turbulent flow of non-Newtonian fluids, smooth channel, for power-law (§ 3.3.1) and Herschel–Bulkley fluids (§ 3.3.2).

For each fluid model, we will obtain expressions for $\tilde{f}$, and thereafter for $\tilde{B}$, which via (2.12) provides the optimal Reynolds number and therefore the optimal radius R for each channel via (2.4) and (2.9). As many expressions for $\tilde{f}$ and $\tilde{B}$ are implicit, finding an optimal channel radius analytically is often impossible. Therefore, we also provide these results in the form of contour plots for the optimisation condition for Re as a function of $\tilde{Q}$ and $\tilde{\tau}_0$, $\tilde{\varepsilon}$ or n.

3.1. *Laminar flow of Newtonian and non-Newtonian fluids*

For laminar flow through a circular channel results in the friction factor (Smink *et al.* 2023)

$$\tilde{f} = \frac{64}{Re\,\psi(\phi, n)^n}, \tag{3.1}$$

where ψ is a dimensionless flow rate that ranges from 0 to 1. For laminar flow, the friction factor is often considered to be independent of the channel wall roughness, but this is only true for $\delta < 0.01$. When the roughness becomes of the order of the channel

size, then the resulting constricted diameter amplifies the friction factor (Liu, Li & Smits 2019). In this section, it is assumed that the relative channel wall roughness is sufficiently small ($\delta < 0.01$), such that the influence of the wall roughness on the friction factor is negligible. For a Herschel–Bulkley fluid, ψ is computed by integration of the velocity field over the channel's cross-section as (Herschel & Bulkley 1926; Chilton & Stainsby 1998; Smink *et al.* 2023)

$$\psi = \frac{(1-\phi)^{(n+1)/n}}{(3n+1)^{-1}} \times \left(\frac{(1-\phi)^2}{3n+1} + \frac{2\phi(1-\phi)}{2n+1} + \frac{\phi^2}{n+1} \right). \tag{3.2}$$

For Bingham fluids ($n = 1$), ψ reduces to (Reiner 1926; Smink *et al.* 2023)

$$\psi = 1 - \frac{4}{3}\phi + \frac{1}{3}\phi^4, \tag{3.3}$$

and for the case of $\tau_0 = 0$ (Newtonian and power-law fluids, $\phi = 0$), ψ further reduces to 1.

Calculation of the optimisation condition results in the following expression for $\tilde{B}$:

$$\tilde{B} = \tilde{f} J(\phi, n), \tag{3.4}$$

where the function $J(\phi, n)$ is defined as

$$J \equiv 1 + \frac{3n}{1 - \dfrac{n\phi}{\psi}\dfrac{\partial\psi}{\partial\phi}}. \tag{3.5}$$

For a Herschel–Bulkley fluid, substitution of ψ from (3.2) into (3.5) results in the following expression for J:

$$J = \frac{3n+1}{\dfrac{6n^3}{(2n+1)(n+1)}\phi^3 + \dfrac{6n^2}{(2n+1)(n+1)}\phi^2 + \dfrac{3n}{2n+1}\phi + 1}. \tag{3.6}$$

For Bingham fluids ($n = 1$), the expression for J reduces to

$$J = \frac{4}{\phi^3 + \phi^2 + \phi + 1}, \tag{3.7}$$

and for non-yield fluids ($\phi = 0$), it reduces to $J = 3n + 1$. Finally, for the yield limit ($\phi = 1$), one obtains $J = 1$.

Substitution of $\tilde{B}$ into (2.12) reduces the optimisation condition to

$$Re^{3(n+1)} = \left(\frac{\pi^3}{8}\right)^{4-3n} a^7 \, \tilde{Q}^{2(n+1)} \left(\frac{\psi(\phi,n)^n}{J(\phi,n)}\right)^{4-3n}. \tag{3.8}$$

Together with (2.18) and (3.1), Re is then explicitly solved for given $\tilde{Q}$, $\tilde{\tau}_0$ and n, providing the optimal radius via (2.4) and (2.9). Figures 8(*a*)–8(*c*) in Appendix E present a contour plot for the optimal Re as function of $\tilde{Q}$ and $\tilde{\tau}_0$ for different values of n. Note that the number of parameters can be reduced even further, by combining $\tilde{Q}$ and Re, to a parameter which is only a function of given $\tilde{\tau}_0$ and n. Then the optimisation condition becomes (Smink *et al.* 2023)

$$\frac{\tilde{R}^3}{\tilde{Q}} = \left(a^3 \frac{\tilde{Q}^2}{Re^3} \right)^{\frac{1}{4-3n}} = \frac{1}{\pi} \left(\left(\frac{3n+1}{n} \right)^n \frac{J(\phi,n)}{\psi(\phi,n)^n} \right)^{1/(n+1)}, \tag{3.9}$$

where the right-hand side is constant for an optimised network. Plotting $\tilde{R}^3/\tilde{Q}$ as function of $\tilde{\tau}_0$ and n gives the contour plot in figure 8(*d*) in Appendix E. This figure can be made for laminar flows because $\tilde{R}^3/\tilde{Q}$ is constant over the entire network, which is highly useful for design of optimised branched fluidic networks, as only one optimisation condition has to be calculated.

3.2. *Turbulent flow of Newtonian fluid, rough and smooth channel*

We now demonstrate that the proposed optimisation method is universal if the friction factor is known, by optimising networks for diverse turbulent flow regimes. For turbulent flow of a Newtonian fluid, the Colebrook-White equation (Colebrook 1939) describes the friction factor for both low- and high-turbulent flow ($Re = [Re_{crit}, \infty)$) in hydraulically smooth and rough pipes using the following implicit equation:

$$f = \left\{ -2.0 \log_{10} \left(\frac{\delta}{3.7} + \frac{2.51}{Re\sqrt{f}} \right) \right\}^{-2}. \tag{3.10}$$

Equation (3.10) underlies the well-known Moody diagram (Moody 1944) as shown in figure 2(*b*). Rewriting (3.10) in terms of the dimensionless numbers gives

$$\tilde{f} = \left\{ -2.0 \log_{10} \left(\frac{1}{3.7} \frac{\pi}{4} \frac{\tilde{\varepsilon} Re}{\tilde{Q}} + \frac{2.51}{Re\sqrt{\tilde{f}}} \right) \right\}^{-2}. \tag{3.11}$$

Differentiation to Re gives

$$\frac{\partial \tilde{f}}{\partial Re} = -\frac{\tilde{f}}{Re} \frac{2 \left(\frac{1}{3.7} \frac{\pi}{4} \frac{\tilde{\varepsilon} Re}{\tilde{Q}} - \frac{2.51}{Re\sqrt{\tilde{f}}} \right)}{\left(\frac{1}{3.7} \frac{\pi}{4} \frac{\tilde{\varepsilon} Re}{\tilde{Q}} + \frac{2.51}{Re\sqrt{\tilde{f}}} \right) \ln \left(\frac{1}{3.7} \frac{\pi}{4} \frac{\tilde{\varepsilon} Re}{\tilde{Q}} + \frac{2.51}{Re\sqrt{\tilde{f}}} \right) - \frac{2.51}{Re\sqrt{\tilde{f}}}}, \tag{3.12}$$

resulting in

$$\tilde{B} = \tilde{f} \left(5 - \frac{2 \left(\frac{1}{3.7} \frac{\pi}{4} \frac{\tilde{\varepsilon} Re}{\tilde{Q}} - \frac{2.51}{Re\sqrt{\tilde{f}}} \right)}{\left(\frac{1}{3.7} \frac{\pi}{4} \frac{\tilde{\varepsilon} Re}{\tilde{Q}} + \frac{2.51}{Re\sqrt{\tilde{f}}} \right) \ln \left(\frac{1}{3.7} \frac{\pi}{4} \frac{\tilde{\varepsilon} Re}{\tilde{Q}} + \frac{2.51}{Re\sqrt{\tilde{f}}} \right) - \frac{2.51}{Re\sqrt{\tilde{f}}}} \right). \tag{3.13}$$

Substituting $\tilde{B}$ into (2.12) enables implicit solving Re for given $\tilde{Q}$. Contour plots of the optimal Re as function $\tilde{Q}$ and $\tilde{\varepsilon}$ are presented in figure 3(*a*). Limit cases of the Colebrook–White equation include complete turbulence (for which Von Kármán's formula applies), turbulence in smooth channels and low-Reynolds-number turbulence in smooth channels (e.g. Blasius' formula). Expressions of the optimal channel radius for these cases are derived in Appendix B.
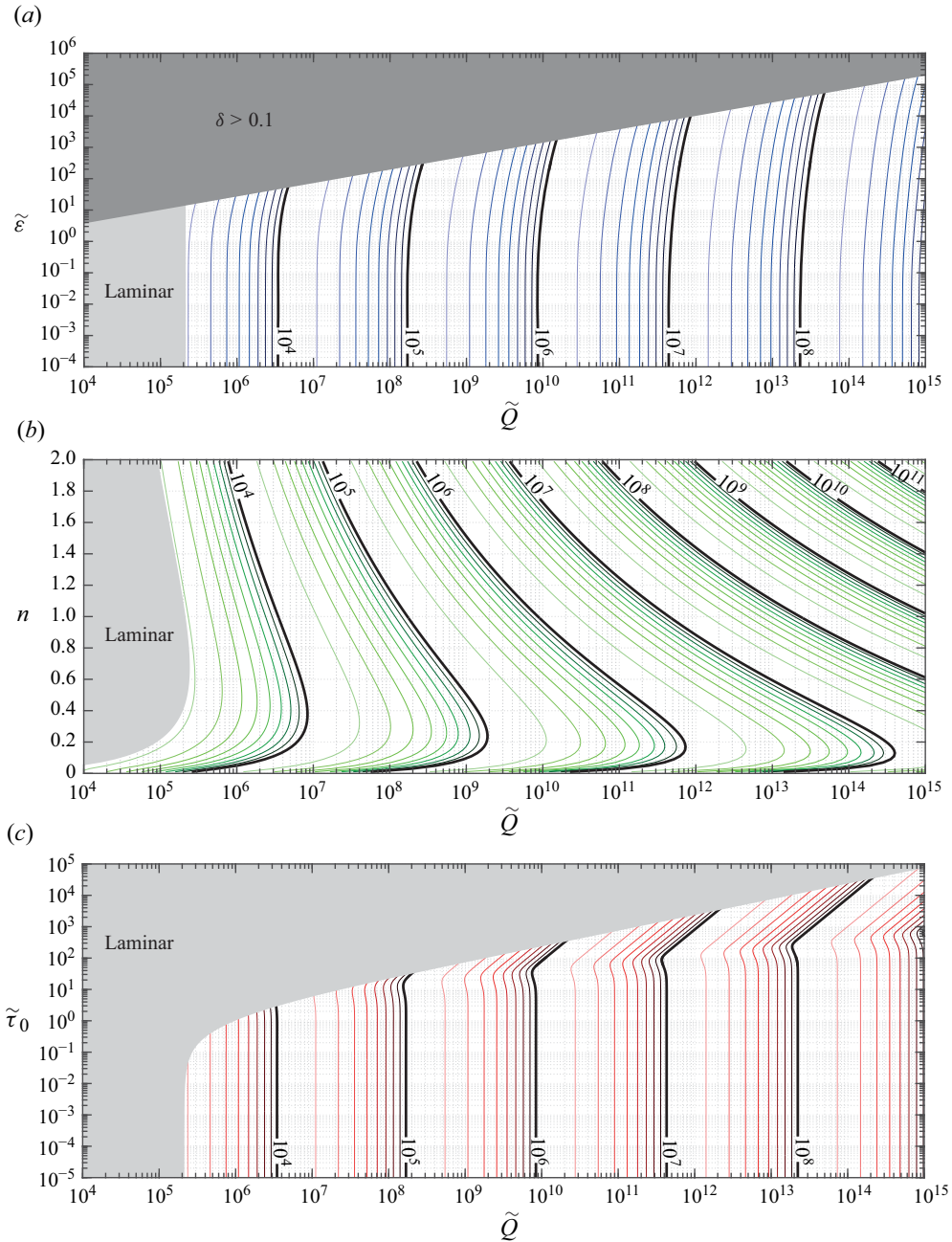
Figure 3. Optimal Re for different fluid models. The colour-scale contour lines represent the Reynolds numbers 2×10^x, 3×10^x, . . .9×10^x with decreasing brightness. (*a*) Contour plot of the optimal Re as function of $\tilde{Q}$ and $\tilde{\varepsilon}$ for a Newtonian fluid in a rough-wall channel. (*b*) Contour plot of the optimal Re as function of $\tilde{Q}$ and n for a power-law fluid in a smooth-wall channel. (*c*) Contour plot of the optimal Re as function of $\tilde{Q}$ and $\tilde{\varepsilon}$ for a Herschel–Bulkley fluid ($n = 1$) in a smooth-wall channel.

3.3. *Turbulent flow of non-Newtonian fluids, smooth channel*

3.3.1. *Power-law fluid*

Turbulent pipe flow of non-Newtonian power-law fluids at low Reynolds numbers in a smooth circular channel ($\varepsilon \to 0$) was analysed by, amongst others, Dodge and Metzner (Dodge & Metzner 1959). They modified the Von Kármán equation for turbulent Newtonian pipe flow, resulting in an implicit relation for the Darcy friction factor f

$$\frac{2}{\sqrt{f}} = \frac{4}{n^{0.75}} \log_{10}\left(Re \left(\frac{f}{4}\right)^{1-n/2}\right) - \frac{0.4}{n^{1.2}}. \tag{3.14}$$

The value of f is shown as a function of Re and n in figure 2(*c*).

Implicit differentiation of $\tilde{f}$ to Re gives

$$\frac{\partial \tilde{f}}{\partial Re} = -\frac{\tilde{f}}{Re}\left(\frac{n^{0.75}\ln 10}{4\sqrt{\tilde{f}}} + 1 - \frac{n}{2}\right)^{-1}, \tag{3.15}$$

resulting in

$$\tilde{B} = \tilde{f}\left(5 + (3n-4)\left(\frac{n^{0.75}\ln 10}{4\sqrt{\tilde{f}}} + 1 - \frac{n}{2}\right)^{-1}\right). \tag{3.16}$$

Here, $\tilde{B}$ is still a function of $\tilde{f}$, which is in turn an implicit function of Re governed by (3.14). Therefore, $\tilde{B}$ is governed by Re and the flow index n. Consequently, with this expression for $\tilde{B}$, the optimal value of Re in a channel can be calculated as function of $\tilde{Q}$ and n. A contour plot for the optimal Reynolds number in a channel is given in figure 3(*b*).

3.3.2. *Herschel–Bulkley fluid*

For a turbulent flow of a Herschel–Bulkley fluid in a smooth circular channel ($\varepsilon \to 0$), Torrance (Garcia & Steffe 1986) developed a relationship for the friction factor. This relation for the Darcy friction factor is given by

$$\frac{2}{\sqrt{\tilde{f}}} = 0.45 - \frac{2.75}{n} + \frac{1.97}{n}\ln(1-\phi) + \frac{1.97}{n}\ln\left(Re\left(\frac{3n+1}{4n}\right)^n\left(\frac{\tilde{f}}{4}\right)^{1-\frac{n}{2}}\right). \tag{3.17}$$

Here, ϕ as given in (2.18) is used in the calculations. Figure 2(*d*) shows f as function of Re for $n = 1.0$ and a range of values of $\tilde{\tau}_0$. The f-Re plots for other values of n are presented in figure 7 in Appendix E.

Implicit differentiation of $\tilde{f}$ to Re leads to

$$\frac{\partial \tilde{f}}{\partial Re} = -\frac{\tilde{f}}{Re}\frac{1 + \dfrac{\phi}{1-\phi}\dfrac{4}{4-3n}}{\dfrac{n}{1.97}\dfrac{1}{\sqrt{\tilde{f}}} + \dfrac{\phi}{1-\phi} + 1 - \dfrac{n}{2}}, \tag{3.18}$$

giving an expression for $\tilde{B}$

$$\tilde{B} = \tilde{f} \left(5 - \frac{4 - 3n + \dfrac{4\phi}{1 - \phi}}{\dfrac{n}{1.97}\dfrac{1}{\sqrt{\tilde{f}}} + \dfrac{\phi}{1 - \phi} + 1 - \dfrac{n}{2}} \right). \tag{3.19}$$

Contour plots for the optimal Reynolds number in a channel as function of $\tilde{\tau}_0$ and $\tilde{Q}$ are given for $n = 1.0$ in figure 3(*c*) and the results for $n = 0.5$ and $n = 1.5$ are provided in figure 9 in Appendix E. An additional fluid model covering laminar and turbulent flow of a Bingham fluid is presented in Appendix C.

4. Scaling of the channel radii

In the literature, many attempts have been made to find the proportionality between the flow rate Q and the channel radius R for optimised networks, in the form of (1.1) (Uylings 1977; Sherman 1981; Woldenberg & Horsfield 1986; Williams *et al.* 2008; Kou *et al.* 2014). In the optimisation method of the present study, only Re and $\tilde{Q}$ contain parameters involving R and Q, while $\tilde{\tau}_0$, $\tilde{\varepsilon}$ and n are independent of R and Q. Therefore, when knowing the proportionality between $\tilde{Q}$ and Re, x can be calculated analytically. However, this only holds if $\tilde{B} \propto Re^{c_1} \tilde{Q}^{c_2}$, which is only true for relatively simple descriptions of f applicable to laminar flows or limit cases of the turbulent regime (e.g. Blasius' formula, Appendix B.3). Therefore, in the following, x will be calculated by locally approximating $\tilde{B}$ by a power function via

$$x = \frac{R}{Q}\frac{\partial Q}{\partial R} = \frac{(4 - 3n)\dfrac{Re}{\tilde{Q}}\dfrac{\partial \tilde{Q}}{\partial Re}}{(2 - n)\dfrac{Re}{\tilde{Q}}\dfrac{\partial \tilde{Q}}{\partial Re} - 1}. \tag{4.1}$$

By calculating the fluid-model-specific $(Re/\tilde{Q})\,\partial \tilde{Q}/\partial Re$, one obtains x in the relevant $(Re, \tilde{\tau}_0, \tilde{\varepsilon}, n)$-space, as shown in figure 4 for the different fluid models (the underlying equations are shown in Appendix D). Known limit cases are shown in black; all coloured results are new. For laminar flow of all treated fluid models, x becomes 3, as expected (Murray 1926*b*; Smink *et al.* 2023) For networks that span ranges of Re for which x is (almost) constant, the value of x is readily used to scale all channels in the network if one optimal diameter is known, using $Q \propto R^x$.

For a Newtonian fluid (figure 4*a*), at the transition from laminar to turbulent flow, x drops quickly from 3 to around 2.5 for hydraulically smooth channels. We find that the low-Re approximations (Blasius, $x = 27/11$, and an empirical relation, $x = 17/7$ (Kou *et al.* 2014)) correspond to the average value of x over their applicable Re-range of the Colebrook–White equation for a smooth channel. Although these approximations and the resulting values of x are valuable for networks that span a limited range of the Reynolds number, the network shown in figure 1(*e*) represents a case where x is not applicable for determination of the optimal channel radii. Here, the optimal network partly corresponds to laminar flow and partly to turbulent flow. As these regimes result in strongly different values of x, as shown by the markers ($\times$) in figure 4(*a*), the so-called Murray's law (Sherman 1981; Stephenson & Lockerby 2016) ($R_0^x = \sum_i R_i^x$, for one branching point) will not hold. Therefore, the optimal radius of each channel must be calculated individually.
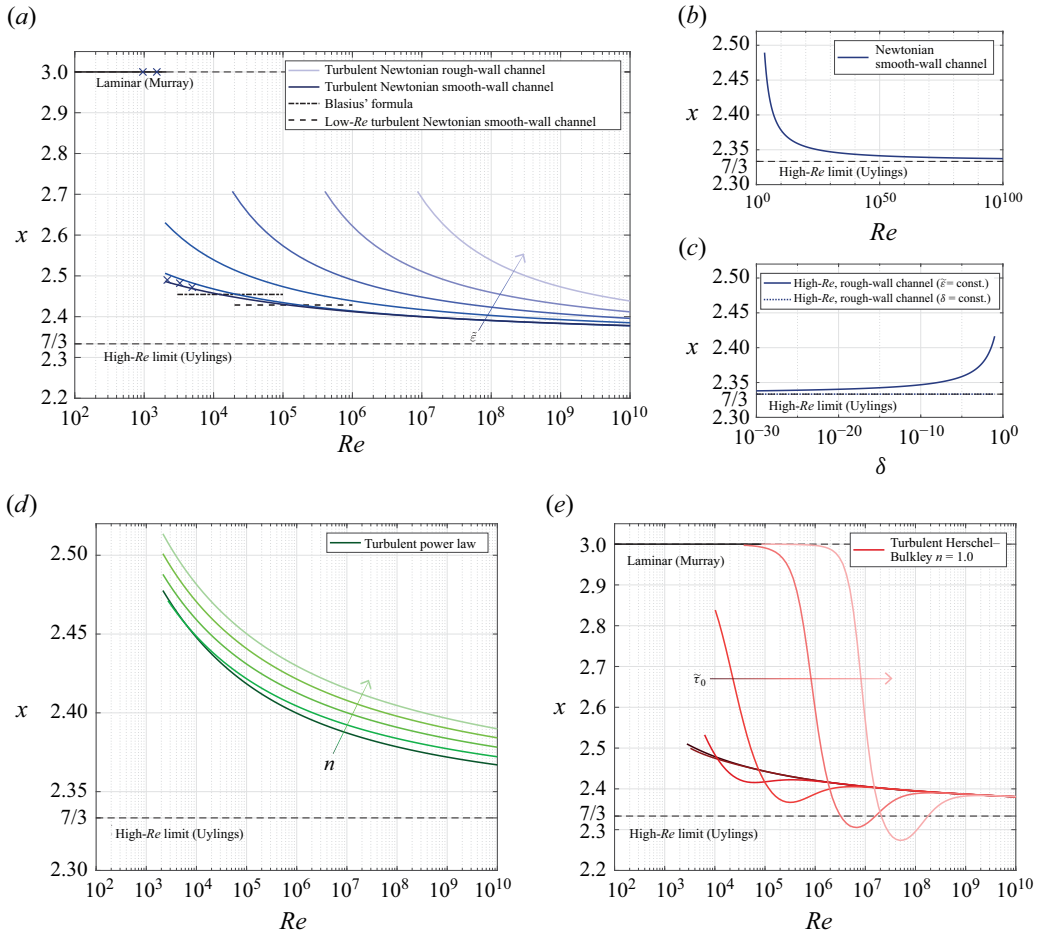
Figure 4. Plot of x (4.1) as function of Re for the different fluid models as discussed in §3. The dashed lines for $x = 3$ and $x = 7/3$ show the expected limit cases for laminar flow and high-turbulent flow, respectively (Uylings 1977). (*a*) Turbulent flow of Newtonian fluids, described by Colebrook–White ($\tilde{\varepsilon} \in [10^{-5}, 10^1, 10^2, 10^3, 10^4, 10^5]$), Blasius' formula (B12) and an empirical relation (B14). The blue $\times$-symbols correspond with the optimised channels in figure 1(*e*), showing that the values for x change significantly for that network. (*b*) Plot of x as function of Re for turbulent flow of a Newtonian fluid in a hydraulically smooth channel, described by (3.10) for the limit of $\tilde{\varepsilon} = 0$. For optimised networks, high-Re turbulent flow in smooth channels will for realistic Re never reach $x = 7/3$. (*c*) Plot of x as function of $\delta = \varepsilon/2R$ for high-Re turbulent flow of a Newtonian fluid in a rough channel, described by (B1). For optimised networks, high-Re turbulent flow in channels with finite roughness will never reach $x = 7/3$. (*d*) Turbulent flow of a power-law fluid (Metzner & Dodge) ($n \in [0.2, 0.4, 1.0, 1.4, 1.8]$). (*e*) Turbulent flow of a Herschel–Bulkley fluid (Torrance) ($\tilde{\tau}_0 \in [0.1, 0.25, 1, 2.5, 10, 25]$ with $n = 1.0$). Plots for $n = 0.5$ and $n = 1.5$ are presented in figure 10 in Appendix E.

Figure 4(*a*) also shows that x increases for increasing wall roughness. The lines are clipped for $\delta = 0.1$, corresponding to $x \approx 2.71$. Analysing the Colebrook–White equation for the smooth-channel limit ($\tilde{\varepsilon} = 0$) shows that, for extremely large Re, x will indeed approach $x = 7/3$, as shown in figure 4(*b*). The high-Re limit for non-zero roughness, however (figure 4(*c*), $\tilde{\varepsilon} = $ const.), shows that $x = 7/3$ will never be reached if a finite value of δ is included in the optimisation process.

When using the Colebrook–White equation, one has to make an assumption about the wall roughness. Figure 4(*a*) shows the results for a fixed dimensionless absolute roughness

$\tilde{\varepsilon}$. One can also choose to fix the relative wall roughness δ, which has often been an implicit assumption in previous works (Uylings 1977; Bejan *et al.* 2000; Kou *et al.* 2014; Stephenson & Lockerby 2016; Zhou *et al.* 2024). Then δ is excluded from the optimisation procedure. Only in this case, it holds for complete turbulence in rough-wall channels that $x = 7/3$ (figure 4*c*, $\delta = $ const.). The assumption of a fixed δ requires that the absolute roughness ε is proportional to the optimised channel radius for every channel in the network. However, many networks consist of a given wall material with uniform absolute roughness ε. Even when there is a changing absolute roughness in the network, the choice for the use of $\tilde{\varepsilon}$ is preferred and then the graphical approach (figure 3*a*) can be used for optimisation of the channel radii.

Figure 4(*d*) shows x for turbulent flow of a power-law fluid in smooth channels. The behaviour of x is similar to that of a Newtonian fluid in a smooth channel, but increases slightly with increasing n. Figure 4(*e*) shows the results for a Herschel–Bulkley fluid ($n = 1.0$), which appears to have a complete transition from $x = 3$ to $x \rightarrow 7/3$, with a remarkable bump in the transition, which is related to the sharp corner around $10^1 < \tilde{\tau}_0 < 10^2$ as observed in the optimisation plot (figure 3*c*). The transition occurs at larger Re for increasing $\tilde{\tau}_0$, and for large Re, all lines converge. Results for $n = 0.5$ and $n = 1.5$ are presented in figure 10 in Appendix E.

The transitional behaviour of x as presented in figure 4 stresses its importance for network optimisation when considering turbulent flow. For domains of Re where x is approximately constant, figure 4 enables making a quick estimation of the optimal channel radii within a network. If one channel within a network has been optimised, then the other channels can be optimised using $Q \propto R^x$. For domains of Re where x clearly non-constant, the full computations of the equations or the use of the graphical approach of figure 3 is required.

5. Synthesis: design of an optimised fluidic network

The framework described in §§ 2, 3 and 4 leads to the following approach for optimisation of branched fluidic networks (such as shown in figure 1*e,f*):

(i) Determine the fluid model and the cost factor α, and calculate $\tilde{\tau}_0$, $\tilde{\varepsilon}$ and n. Calculate $\tilde{Q}$ for all the to be optimised channels (§ 2).
(ii) Determine the optimal radius R in one channel.

    (a) First, determine the optimal Re by one of the following options:

        – Read Re from an optimisation contour plot (e.g. Figure 3*a*) for given $\tilde{Q}$.
        – Calculate $\tilde{B}(\tilde{f}, Re, \tilde{Q}, \tilde{\tau}_0, \tilde{\varepsilon}, n)$ via (2.13) and then solve (2.12) for Re for given $\tilde{Q}$.

    (b) Subsequently, calculate R from the calculated Re by using (2.4).

(iii) Obtain all channel radii:

    – By repeating step 2 for each channel, or
    – by obtaining x from figure 4 and calculating all channel radii using $Q \propto R^x$. This option only applies if x is (almost) constant over the applicable range of Re.
(iv) Calculate the optimal location of the branching points (Appendix A.1).

This approach is illustrated by an example of the optimisation of a fluidic network with turbulent flow of a Newtonian fluid in rough-wall channels, presented in Appendix F.

6. Conclusion

A unifying design procedure for optimisation of branched fluidic networks was presented. The optimal channel radius is obtained by minimising the power consumption for maintaining the flow and minimising the volume simultaneously, which is carried out for all channel segments individually. The approach is applicable to every flow configuration for which the Darcy friction factor is available, even for non-power-law or implicit formulations.

Network optimisation was carried out for the parameter space spanned by the Reynolds number (laminar and turbulent flows), the wall roughness and for different rheologies. This parameter space is widely applicable to e.g. heat exchangers or (inertial) microfluidics, but was hardly covered in the literature, as shown in figure 1(*a*,*b*). First, the entire optimisation problem is non-dimensionalised in terms of Re, $\tilde{Q}$, $\tilde{\tau}_0$, $\tilde{\varepsilon}$ and n. For every channel, the optimal Reynolds number and the optimal channel radius are obtained as a function of the dimensionless flow rate $\tilde{Q}$. To minimise the required mathematical analysis, graphs are presented that readily provide the optimal Reynolds number for every fluid model.

Subsequently, the value of x in the proportionality $Q \propto R^x$ was evaluated for the full parameter space of the Reynolds number and channel roughness for different fluid rheologies. The well-known limit values $x = 3$ for laminar flow and $x = 7/3$ for high-Re turbulence were recovered (Uylings 1977; Bejan *et al.* 2000; Kou *et al.* 2014; Stephenson & Lockerby 2016; Zhou *et al.* 2024). However, as the latter value is hardly reached in practice, the intermediate values of x were calculated and plotted. This revealed in which case the entire network can be optimised based on one optimal channel radius, and in which case all radii must be optimised individually. Finally, a design procedure of optimised fluidic networks that incorporates all aforementioned elements was presented.

Our unifying approach for optimisation of fluidic networks can be extended to other configurations with known friction factors, including non-circular cross-sections, bended pipes, bubbly flows, porous walls (Miguel 2018), porous media (MacDonald *et al.* 1991) or slip flow (Morini & Spiga 1998). As such, it enables optimisation of many realistically encountered configurations in nature and engineering.

Declaration of interests. The authors report no conflict of interest.

Appendix A. Details on optimisation of a fluidic branching

A.1 *Optimal branching point location*

To minimise the power in a network, the location of the branching point $\boldsymbol{x}$ must be chosen. If the channel radii are optimised according to (2.12), this is the same as minimising the total volume within the channels. Differentiation of the total power P (2.1) to $\boldsymbol{x}$ results in

$$\nabla_{\boldsymbol{x}} P = \sum_{i=0}^{N} \left(\left| \frac{\mathrm{d}p}{\mathrm{d}z} \right|_i Q_i + \alpha \pi R_i^2 \right) \nabla L_i = \boldsymbol{0}, \quad i = 0, 1, \ldots, N, \tag{A1}$$

where we define

$$\boldsymbol{e}_{i,*} \equiv (\nabla L_i)_* = \frac{\boldsymbol{x}_* - \boldsymbol{x}_i}{|\boldsymbol{x}_* - \boldsymbol{x}_i|}. \tag{A2}$$

Here, the subscript i indicates the index of the channel, and the subscript $*$ indicates an optimised parameter.

Substituting the optimisation condition for the channel radii (2.12) results in the optimisation condition of the branching point $x = x_*$ (for a full derivation, see Smink *et al.* (2023))

$$\sum_{i=0}^{N} \left(R_{i,*}^2 \frac{2f + B}{B} e_{i,*} \right) = 0, \quad i = 0, 1, \ldots, N. \tag{A3}$$

Alternatively, we can rewrite (A3) in terms of dimensionless numbers

$$\sum_{i=0}^{N} \left(\frac{\tilde{Q}^{2-n}}{Re} \right)^{\frac{2}{4-3n}} \frac{2\tilde{f} + \tilde{B}}{\tilde{B}} e_{i,*} = 0, \quad i = 0, 1, \ldots, N. \tag{A4}$$

Equation (A4) requires the optimal Reynolds number and corresponding $\tilde{f}$, $\tilde{B}$ and $\tilde{Q}$ for each channel for computation of the optimal branching point location. It is an implicit equation, such that the coordinates of x_* are solved by simple numerical methods, providing the lengths of the channels L_i. The resulting x_* determines a network that is optimised both with respect to the channel radii (2.12) and the channel lengths (A4).

A.2 *Governing dimensionless numbers*

Scaling of the problem for calculation of the optimisation condition for the channel radii is investigated using the Buckingham-Pi theorem. The goal is to find a non-dimensionalisation of the radius and the dimensionless parameters where it depends on. In this problem, the following 8 independent parameters are relevant: the channel radius R in m, the flow rate Q in m^3 s^{-1}, the fluid density ρ in kg m^{-3}, the viscosity index μ' in Pa s^n, the cost factor α in W m^{-3}, the yield stress τ_0 in Pa, the channel absolute roughness ε in m and the flow index n. In these parameters, 3 independent physical dimensions are present. We choose ρ, μ' and α to scale this problem, which are suitable for the scaling. We will end up with 5 dimensionless parameters, where n is one of them.

In mathematical terms, the problem is then

$$R = g(\rho, \mu', \alpha, Q, \tau_0, \varepsilon, n), \tag{A5}$$

where scaling of the problem results in

$$\tilde{R} = \tilde{g}(\tilde{Q}, \tilde{\tau}_0, \tilde{\varepsilon}, n), \tag{A6}$$

with

$$\tilde{R} \equiv \frac{R}{\rho^{-\frac{1}{2}} \mu'^{\frac{3}{2(n+1)}} \alpha^{\frac{n-2}{2(n+1)}}}, \quad \tilde{Q} \equiv \frac{Q}{\rho^{-\frac{3}{2}} \mu'^{\frac{7}{2(n+1)}} \alpha^{\frac{3n-4}{2(n+1)}}},$$

$$\tilde{\tau}_0 \equiv \frac{\tau_0}{\mu'^{\frac{1}{n+1}} \alpha^{\frac{n}{n+1}}} \quad \text{and} \quad \tilde{\varepsilon} \equiv \frac{\varepsilon}{\rho^{-\frac{1}{2}} \mu'^{\frac{3}{2(n+1)}} \alpha^{\frac{n-2}{2(n+1)}}}. \tag{A7}$$

For convenience, the Reynolds number will be used instead of $\tilde{R}$. This choice simplifies the calculations and provides direct characterisation of the flow in the channels. Expressed in dimensionless groups, the Reynolds number (2.4) becomes

$$Re = a(n) \frac{\tilde{Q}^{2-n}}{\tilde{R}^{4-3n}}, \tag{A8}$$

where $a(n)$ is defined as

$$a(n) \equiv \frac{8}{\pi^{2-n}} \left(\frac{n}{3n+1} \right)^n.$$ (A9)

In the end, a network can be described by the dimensionless numbers Re, $\tilde{Q}$, $\tilde{\tau}_0$, $\tilde{\varepsilon}$ and n. All parameters except for R and Q are fluid or system parameters, which are constant in a network. In a branched fluidic network, Q can change from channel to channel. Therefore, for design procedure purposes, it is convenient that Re and $\tilde{Q}$ are the only flow-rate-dependent dimensionless numbers.

Therefore, the optimisation problem is reduced to the dimensionless dependency

$$Re = \tilde{g}_1(\tilde{Q}, \tilde{\tau}_0, \tilde{\varepsilon}, n).$$ (A10)

For $n = 1$, the dimensionless numbers reduce to

$$Re = \frac{2}{\pi} \frac{\rho Q}{\mu' R}, \quad \tilde{Q} = \frac{\alpha^{\frac{1}{4}} \rho^{\frac{3}{2}} Q}{\mu'^{\frac{7}{4}}}, \quad \tilde{\tau}_0 = \frac{\tau_0}{(\mu'\alpha)^{\frac{1}{2}}} \quad \text{and} \quad \tilde{\varepsilon} = \frac{\rho^{\frac{1}{2}} \alpha^{\frac{1}{4}} \varepsilon}{\mu'^{\frac{3}{4}}}.$$ (A11)

For given fluid, flow and system properties, an optimal channel radius can be calculated from the obtained optimal Reynolds number.

A.3 *Mapping from 4 to 5 variables for f*

The friction factor f commonly depends on the Reynolds number Re, the Hedström number He, the relative wall roughness δ and the flow index n. These are 4 independent dimensionless groups. In the optimisation procedure, the following 5 dimensionless numbers are used (for details, see Appendix A.2): Re, $\tilde{Q}$, $\tilde{\tau}_0$, $\tilde{\varepsilon}$ and n. Because the friction factor will now be described by 5 instead of 4 dimensionless numbers, a curve in the 5-variable space exists along which f is constant. The direction of that curve is locally described by the vector $\boldsymbol{\beta} = (\beta_1, \beta_2, \beta_3, \beta_4, \beta_5)^T$. Therefore, the inner product of this vector with the gradient of the original variables $\boldsymbol{F} = (Re, He, \delta, n)^T$ to the new variables $\tilde{\boldsymbol{F}} = (Re, \tilde{Q}, \tilde{\tau}_0, \tilde{\varepsilon}, n)^T$ must be zero. In that case, Re, He, δ and n are constant along the direction of $\boldsymbol{\beta}$. This results in the following 4 equations:

$$\sum_{j=1}^{5} \frac{\partial F_i}{\partial \tilde{F}_j} \beta_j = 0, \qquad i = 1, 2, 3, 4,$$ (A12)

which are sufficient to define the direction of the vector $\boldsymbol{\beta}$ while choosing its arbitrary length by conveniently choosing $\beta_2 = 1$. Solving (A12) results in $\beta_1 = 0$, $\beta_3 = -(2n/(4-3n)) \, \tilde{\tau}_0 \beta_2/\tilde{Q}$, $\beta_4 = ((2-n)/(4-3n)) \, \tilde{\varepsilon}\beta_2/\tilde{Q}$ and $\beta_5 = 0$.

The function of f will be restricted in the new parameter space by

$$\sum_{j=1}^{5} \frac{\partial f}{\partial \tilde{F}_j} \beta_j = 0.$$ (A13)

Substituting the obtained coefficients $\boldsymbol{\beta}$ results in the following expression:

$$\tilde{Q} \frac{\partial f}{\partial \tilde{Q}} - \frac{2n}{4-3n} \tilde{\tau}_0 \frac{\partial f}{\partial \tilde{\tau}_0} + \frac{2-n}{4-3n} \tilde{\varepsilon} \frac{\partial f}{\partial \tilde{\varepsilon}} = 0,$$ (A14)

which provides the curve along which f is constant in the new parameter space.

Appendix B. Specific cases of turbulent flow of Newtonian fluid, rough and smooth channel

B.1 *Complete turbulence, rough channel*

For sufficiently large Reynolds numbers, the friction factor corresponding to fully developed turbulent flow in a circular channel can quite accurately be described by Von Kármán's formula (Haaland 1983), which holds for rough channels in the limit of high Reynolds numbers

$$ f = \left\{ -2.0 \log_{10} \left(\frac{\delta}{3.7} \right) \right\}^{-2}. \tag{B1} $$

This equation is a limit case of the Colebrook–White equation, valid for the complete turbulent regime ($Re > 3500/\delta$) (Moody 1944). In terms of $\tilde{\varepsilon}$, $\tilde{Q}$ and Re, f becomes

$$ \tilde{f} = \left\{ -2.0 \log_{10} \left(\frac{1}{3.7} \frac{\pi}{4} \frac{\tilde{\varepsilon} Re}{\tilde{Q}} \right) \right\}^{-2}. \tag{B2} $$

Differentiation to Re results in

$$ \frac{\partial \tilde{f}}{\partial Re} = -\frac{\tilde{f}}{Re} \frac{2}{\ln \left(\dfrac{1}{3.7} \dfrac{\pi}{4} \dfrac{\tilde{\varepsilon} Re}{\tilde{Q}} \right)}, \tag{B3} $$

resulting in

$$ \tilde{B} = \tilde{f} \left(5 - \frac{2}{\ln \left(\dfrac{1}{3.7} \dfrac{\pi}{4} \dfrac{\tilde{\varepsilon} Re}{\tilde{Q}} \right)} \right). \tag{B4} $$

Contour plots of the optimal Re as function $\tilde{Q}$ and $\tilde{\varepsilon}$ are presented in figure 3(*a*), for the high-$\tilde{\varepsilon}$ limit.

B.2 *Turbulence, smooth channel*

For a smooth-wall channel ($\varepsilon \to 0$), the Colebrook–White equation (Colebrook 1939) reduces to

$$ \tilde{f} = \left\{ -2.0 \log_{10} \left(\frac{2.51}{Re\sqrt{\tilde{f}}} \right) \right\}^{-2}. \tag{B5} $$

Differentiation to Re gives

$$ \frac{\partial \tilde{f}}{\partial Re} = \frac{\tilde{f}}{Re} \frac{2}{\ln \left(\dfrac{2.51}{Re\sqrt{\tilde{f}}} \right) - 1}, \tag{B6} $$
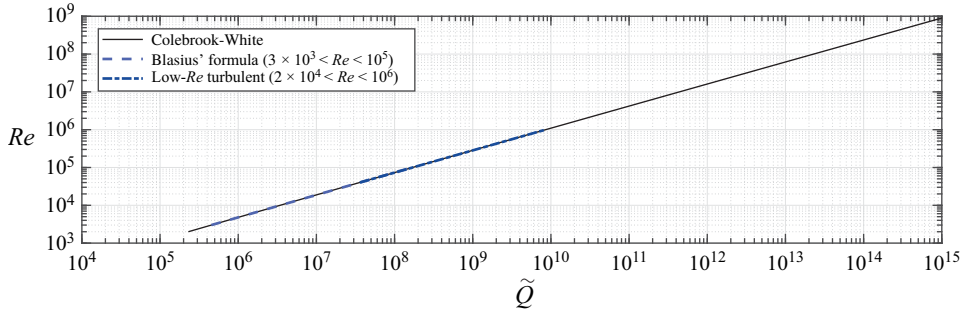
Figure 5. Optimal Re as function of $\tilde{Q}$ for a Newtonian fluid in a smooth-wall channel according to the Colebrook–White equation, together with the Blasius' formula and a low-Re turbulent approximation.

resulting in

$$\tilde{B} = \tilde{f}\left(5 + \cfrac{2}{\ln\left(\cfrac{2.51}{Re\sqrt{\tilde{f}}}\right) - 1}\right). \tag{B7}$$

Figure 5 shows the optimisation curve for Re as function of $\tilde{Q}$. This result corresponds to the contour plot of the optimal Re as function $\tilde{Q}$ and $\tilde{\varepsilon}$ as presented in figure 3(*a*) for $\tilde{\varepsilon} \to 0$.

B.3 *Low-Reynolds-number turbulence, smooth channel*

Power-law approximations for the friction factor have been established for turbulent flows in smooth channels ($\varepsilon \to 0$), for specific and limited ranges of the Reynolds number, in the general form

$$\tilde{f} = \frac{c_1}{Re^{c_2}}, \tag{B8}$$

with c_1 and c_2 being two relation-dependent constants. This is an explicit expression for $\tilde{f}$ as function of Re, resulting in $\tilde{B}$ being

$$\tilde{B} = (5 - c_2)\tilde{f} = \frac{c_1(5 - c_2)}{Re^{c_2}}. \tag{B9}$$

For Newtonian fluids, the optimisation condition (2.12) reduces to

$$\tilde{B}\,Re^7 = \frac{1024}{\pi^4}\,\tilde{Q}^4, \tag{B10}$$

which can for this case be rewritten to

$$Re = \left(\frac{1024}{c_1(5 - c_2)}\right)^{\frac{1}{7-c_2}}\left(\frac{\tilde{Q}}{\pi}\right)^{\frac{4}{7-c_2}}. \tag{B11}$$

Blasius' formula (Blasius 1912, 1913), which is valid for $3 \times 10^3 < Re < 10^5$, is given by

$$\tilde{f} = \frac{0.3164}{Re^{\frac{1}{4}}}, \tag{B12}$$

resulting in the optimisation condition

$$Re = 2.629 \left(\frac{\tilde{Q}}{\pi} \right)^{\frac{16}{27}}. \tag{B13}$$

An empirical relation valid for turbulent flows at intermediate Reynolds numbers ($2 \times 10^4 < Re < 10^6$) (Bejan 2013) is given by

$$\tilde{f} = \frac{0.184}{Re^{\frac{1}{5}}}, \tag{B14}$$

resulting in the optimisation condition

$$Re = 2.822 \left(\frac{\tilde{Q}}{\pi} \right)^{\frac{10}{17}}. \tag{B15}$$

These explicit expressions for the optimal Re as function of $\tilde{Q}$ are shown in figure 5 for Blasius' formula (B12) and low-Re turbulence (B14), revealing perfect coincidence with the more general Colebrook–White solution for smooth channels.

Appendix C. Laminar and low-Reynolds-number turbulent flow of Bingham fluid, smooth channel

Considering a turbulent flow of a Bingham fluid in a circular pipe brings to empirical and numerical approximations for the friction factor f. Darby *et al.* (Darby, Mun & Boger 1992) developed an empirical curve-fit equation, composed of the following structure:

$$f = \left(f_L^{\chi_1} + f_T^{\chi_1} \right)^{1/\chi_1}$$

$$f_T = 4 \times 10^{\chi_2} Re^{-0.193}$$

$$\chi_1 = 1.7 + \frac{4 \times 10^5}{Re}$$

$$\chi_2 = -1.47(1 + 0.146 \exp(-2.9 \times 10^{-5} He)), \tag{C1}$$

where f_L is the laminar friction factor as determined from the Buckingham–Reiner (Reiner 1926) equation ((2.18), (3.1) and (3.3) combined).

In the new set of dimensionless numbers, the friction factor $\tilde{f}$ becomes

$$\tilde{f} = \left(\tilde{f}_L^{\tilde{\chi}_1} + \tilde{f}_T^{\tilde{\chi}_1} \right)^{1/\tilde{\chi}_1}$$

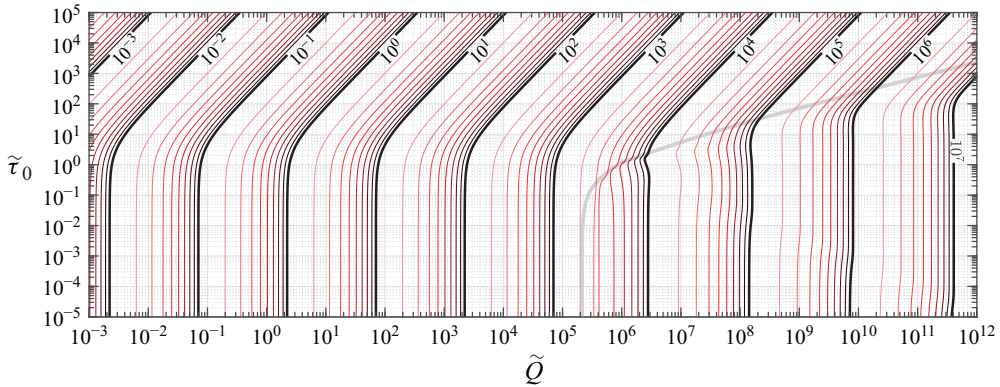$$\tilde{f}_T = 4 \times 10^{\tilde{\chi}_2} Re^{-0.193}$$

Figure 6. Contour plot of the optimal Reynolds number as a function of $\tilde{Q}$ and $\tilde{\tau}_0$, for both laminar and low-Reynolds-number turbulent flow of a Bingham fluid (C1). The red-scale contour lines represent the Reynolds numbers 2×10^x, 3×10^x, ...9×10^x with decreasing brightness. The thick grey line represents the critical Reynolds number.

$$\tilde{\chi}_1 = 1.7 + \frac{4 \times 10^5}{Re}$$

$$\tilde{\chi}_2 = -1.47 \left(1 + 0.146 \exp \left(-2.9 \times 10^{-5} \frac{16}{\pi^2} \frac{\tilde{Q}^2}{Re^2} \tilde{\tau}_0 \right) \right). \tag{C2}$$

Implicit differentiation of $\tilde{f}$ to Re results in the following expression:

$$\frac{\partial \tilde{f}}{\partial Re} = \frac{\tilde{f}}{Re} \left[\frac{1.7 - \tilde{\chi}_1}{\tilde{\chi}_1} \left(\left(\frac{\tilde{f}_L}{\tilde{f}} \right)^{\tilde{\chi}_1} \ln \tilde{f}_L + \left(\frac{\tilde{f}_T}{\tilde{f}} \right)^{\tilde{\chi}_1} \ln \tilde{f}_T - \ln \tilde{f} \right) \right.$$
$$\left. + (J(\phi) - 5) \left(\frac{\tilde{f}_L}{\tilde{f}} \right)^{\tilde{\chi}_1} + \left(\ln(10) Re \frac{\partial \tilde{\chi}_2}{\partial Re} - 0.193 \right) \left(\frac{\tilde{f}_T}{\tilde{f}} \right)^{\tilde{\chi}_1} \right], \tag{C3}$$

where

$$\frac{\partial \tilde{\chi}_2}{\partial Re} = -1.99 \times 10^{-4} \times \frac{\tilde{Q}^2 \tilde{\tau}_0}{\pi^2 Re^3} \exp \left(-4.64 \times 10^{-4} \frac{\tilde{Q}^2 \tilde{\tau}_0}{\pi^2 Re^2} \right) \tag{C4}$$

resulting in

$$\tilde{B} = \tilde{f} \left(5 + \frac{Re}{\tilde{f}} \frac{\partial \tilde{f}}{\partial Re} \right). \tag{C5}$$

The set of equations for this fluid model is relatively complex, but has as benefit that it covers both the laminar and turbulent regimes. The contour plot in figure 6 gives the optimal Reynolds number in a channel for given $\tilde{\tau}_0$ and $\tilde{Q}$.

Appendix D. Approximation of x for different fluid models

In network optimisation, many attempts have been made to find the proportionality between the flow rate Q and the channel radius R for optimised networks, in the following form:

1011 A42-22

$$Q \propto R^x. \tag{D1}$$

In the optimisation method of the present study, only Re and $\tilde{Q}$ contain parameters involving R and Q, whereas $\tilde{\tau}_0$, $\tilde{\varepsilon}$ and n are independent of R and Q. Therefore, when knowing the proportionality between $\tilde{Q}$ and Re, one can obtain x using (D1). However, this is only possible if $\tilde{B} \propto Re^{c_1} \tilde{Q}^{c_2}$. However, in most of the cases (except for e.g. Blasius' formula), this is not true. Therefore, x is calculated by locally approximating $\tilde{B}$ by a power function using

$$x = \frac{R}{Q}\frac{\partial Q}{\partial R} = \frac{(4-3n)\dfrac{Re}{\tilde{Q}}\dfrac{\partial \tilde{Q}}{\partial Re}}{(2-n)\dfrac{Re}{\tilde{Q}}\dfrac{\partial \tilde{Q}}{\partial Re} - 1} = 3 - \frac{2\dfrac{Re}{\tilde{Q}}\dfrac{\partial \tilde{Q}}{\partial Re} - 3}{(2-n)\dfrac{Re}{\tilde{Q}}\dfrac{\partial \tilde{Q}}{\partial Re} - 1}, \tag{D2}$$

where $(Re/\tilde{Q})\partial \tilde{Q}/\partial Re$ is derived to be

$$
\begin{aligned}
\frac{Re}{\tilde{Q}}\frac{\partial \tilde{Q}}{\partial Re} = &-\left[\left((4-3n)\frac{Re}{\tilde{B}}\left(\frac{\partial \tilde{B}}{\partial Re}\right)_{\tilde{f},\tilde{Q},\phi} - 4\frac{\phi}{\tilde{B}}\left(\frac{\partial \tilde{B}}{\partial \phi}\right)_{\tilde{f},\tilde{Q},Re} + 7\right)\left(1 + \frac{\phi}{\tilde{f}}\left(\frac{\partial \tilde{f}}{\partial \phi}\right)_{\tilde{Q},Re}\right)\right. \\
&+ \left.\left(\frac{\tilde{f}}{\tilde{B}}\left(\frac{\partial \tilde{B}}{\partial \tilde{f}}\right)_{\tilde{Q},\phi,Re} - \frac{\phi}{\tilde{B}}\left(\frac{\partial \tilde{B}}{\partial \phi}\right)_{\tilde{f},\tilde{Q},Re}\right)\left((4-3n)\frac{Re}{\tilde{f}}\left(\frac{\partial \tilde{f}}{\partial Re}\right)_{\tilde{Q},\phi} - 4\frac{\phi}{\tilde{f}}\left(\frac{\partial \tilde{f}}{\partial \phi}\right)_{\tilde{Q},Re}\right)\right] \\
&\times \left[\left(2n\frac{\phi}{\tilde{B}}\left(\frac{\partial \tilde{B}}{\partial \phi}\right)_{\tilde{f},\tilde{Q},Re} + (4-3n)\frac{\tilde{Q}}{\tilde{B}}\left(\frac{\partial \tilde{B}}{\partial \tilde{Q}}\right)_{\tilde{f},\phi,Re} - 2(n+1)\right)\left(1 + \frac{\phi}{\tilde{f}}\left(\frac{\partial \tilde{f}}{\partial \phi}\right)_{\tilde{Q},Re}\right)\right. \\
&+ \left.\left(\frac{\tilde{f}}{\tilde{B}}\left(\frac{\partial \tilde{B}}{\partial \tilde{f}}\right)_{\tilde{Q},\phi,Re} - \frac{\phi}{\tilde{B}}\left(\frac{\partial \tilde{B}}{\partial \phi}\right)_{\tilde{f},\tilde{Q},Re}\right)\left(2n\frac{\phi}{\tilde{f}}\left(\frac{\partial \tilde{f}}{\partial \phi}\right)_{\tilde{Q},Re} + (4-3n)\frac{\tilde{Q}}{\tilde{f}}\left(\frac{\partial \tilde{f}}{\partial \tilde{Q}}\right)_{\phi,Re}\right)\right]^{-1}.
\end{aligned} \tag{D3}
$$

Equation (D3) is an expression containing 7 differentials of $\tilde{B}$ or $\tilde{f}$ to Re, ϕ, $\tilde{f}$ or $\tilde{Q}$. All differentials can be calculated with keeping the parameters in subscript fixed. The differentials have to be calculated for every flow model separately. The calculated value for x is only valid around its corresponding point in the $(Re, \tilde{\tau}_0, \tilde{\varepsilon}, n)$-space with a limited range depending on the change in x. Expressions for the differentials for the fluid models presented in the following sections.

D.1 *Laminar flow of a Newtonian, power-law, Bingham and Herschel–Bulkley fluids*

For a laminar flow, the friction factor was found to be

$$\tilde{f} = \frac{64}{Re\,\psi(\phi, n)^n}, \tag{D4}$$

resulting in an expression for $\tilde{B}$ being

$$\tilde{B} = \tilde{f}J(\phi, n), \tag{D5}$$

where $J(\phi, n)$ is defined as

$$J \equiv 1 + \frac{3n}{1 - \dfrac{n\phi}{\psi}\dfrac{\partial \psi}{\partial \phi}}. \tag{D6}$$

Differentiation provides the needed differentials in (D3), resulting in the expression for x (D2)

$$\frac{\tilde{f}}{\tilde{B}}\left(\frac{\partial \tilde{B}}{\partial \tilde{f}}\right)_{\tilde{Q},\phi,Re} = 1, \qquad \frac{Re}{\tilde{B}}\left(\frac{\partial \tilde{B}}{\partial Re}\right)_{\tilde{f},\tilde{Q},\phi} = 0, \qquad \frac{\phi}{\tilde{B}}\left(\frac{\partial \tilde{B}}{\partial \phi}\right)_{\tilde{f},\tilde{Q},Re} = \frac{\phi}{J}\frac{\partial J}{\partial \phi},$$

$$\frac{\tilde{Q}}{\tilde{B}}\left(\frac{\partial \tilde{B}}{\partial \tilde{Q}}\right)_{\tilde{f},\phi,Re} = 0, \qquad \frac{Re}{\tilde{f}}\left(\frac{\partial \tilde{f}}{\partial Re}\right)_{\tilde{Q},\phi} = -1, \qquad \frac{\phi}{\tilde{f}}\left(\frac{\partial \tilde{f}}{\partial \phi}\right)_{\tilde{Q},Re} = -\frac{n\phi}{\psi}\frac{\partial \psi}{\partial \phi},$$

$$\frac{\tilde{Q}}{\tilde{f}}\left(\frac{\partial \tilde{f}}{\partial \tilde{Q}}\right)_{\phi,Re} = 0. \tag{D7}$$

Substituting everything into (D3) results in $(Re/\tilde{Q})\,\partial \tilde{Q}/\partial Re = 3/2$, resulting in $x = 3$. This holds for laminar flow of all treated fluid models.

D.2 *Turbulent flow of Newtonian fluid, rough and smooth channel*

A turbulent flow of a Newtonian fluid in a rough or smooth channel can be described by the Colebrook–White equation (Colebrook 1939), which is in the applied non-dimensionalisation

$$\tilde{f} = \left\{-2.0\log_{10}\left(k_1 + k_2\right)\right\}^{-2}, \tag{D8}$$

with

$$k_1 \equiv \frac{1}{3.7}\frac{\pi}{4}\frac{\tilde{\varepsilon}Re}{\tilde{Q}}, \tag{D9}$$

$$k_2 \equiv \frac{2.51}{\sqrt{\tilde{f}}\,Re}. \tag{D10}$$

Differentiation provides the needed differentials in (D3)

$$\frac{\tilde{f}}{\tilde{B}}\left(\frac{\partial \tilde{B}}{\partial \tilde{f}}\right)_{\tilde{Q},\phi,Re} = 1 - \frac{\tilde{f}}{\tilde{B}}\left[\frac{2k_1 k_2 \ln(k_1+k_2) - k_2^2}{[(k_1+k_2)\ln(k_1+k_2) - k_2]^2}\right],$$

$$\frac{Re}{\tilde{B}}\left(\frac{\partial \tilde{B}}{\partial Re}\right)_{\tilde{f},\tilde{Q},\phi} = \frac{\tilde{f}}{\tilde{B}}\left[\frac{-8k_1 k_2 \ln(k_1+k_2) + 2k_1^2 + 2k_2^2}{[(k_1+k_2)\ln(k_1+k_2) - k_2]^2}\right], \qquad \frac{\phi}{\tilde{B}}\left(\frac{\partial \tilde{B}}{\partial \phi}\right)_{\tilde{f},\tilde{Q},Re} = 0,$$

$$\frac{\tilde{Q}}{\tilde{B}}\left(\frac{\partial \tilde{B}}{\partial \tilde{Q}}\right)_{\tilde{f},\phi,Re} = \frac{\tilde{f}}{\tilde{B}}\left[\frac{4k_1 k_2 \ln(k_1+k_2) - 2k_1^2}{[(k_1+k_2)\ln(k_1+k_2) - k_2]^2}\right],$$

$$\frac{Re}{\tilde{f}}\left(\frac{\partial \tilde{f}}{\partial Re}\right)_{\tilde{Q},\phi} = \frac{2(k_2 - k_1)}{(k_1+k_2)\ln(k_1+k_2) - k_2}, \qquad \frac{\phi}{\tilde{f}}\left(\frac{\partial \tilde{f}}{\partial \phi}\right)_{\tilde{Q},Re} = 0,$$

$$\frac{\tilde{Q}}{\tilde{f}}\left(\frac{\partial \tilde{f}}{\partial \tilde{Q}}\right)_{\phi,Re} = \frac{2k_1}{(k_1+k_2)\ln(k_1+k_2) - k_2}. \tag{D11}$$

D.2.1 *Complete turbulent flow of Newtonian fluid, rough channel*

For sufficiently large Reynolds numbers, the friction factor corresponding to complete turbulence in a circular channel can accurately be described by Von Kármán's formula (Haaland 1983)

$$f = \left\{ -2.0 \log_{10} \left(\frac{1}{3.7} \frac{\pi}{4} \frac{\tilde{\varepsilon} Re}{\tilde{Q}} \right) \right\}^{-2}. \tag{D12}$$

Differentiation provides the needed differentials in (D3)

$$\frac{\tilde{f}}{\tilde{B}} \left(\frac{\partial \tilde{B}}{\partial \tilde{f}} \right)_{\tilde{Q}, \phi, Re} = 1, \quad \frac{Re}{\tilde{B}} \left(\frac{\partial \tilde{B}}{\partial Re} \right)_{\tilde{f}, \tilde{Q}, \phi} = \frac{\tilde{f}}{\tilde{B}} \frac{2}{\left(\ln \left(\frac{1}{3.7} \frac{\pi}{4} \frac{\tilde{\varepsilon} Re}{\tilde{Q}} \right) \right)^2},$$

$$\frac{\phi}{\tilde{B}} \left(\frac{\partial \tilde{B}}{\partial \phi} \right)_{\tilde{f}, \tilde{Q}, Re} = 0, \quad \frac{\tilde{Q}}{\tilde{B}} \left(\frac{\partial \tilde{B}}{\partial \tilde{Q}} \right)_{\tilde{f}, \phi, Re} = \frac{\tilde{f}}{\tilde{B}} \frac{-2}{\left(\ln \left(\frac{1}{3.7} \frac{\pi}{4} \frac{\tilde{\varepsilon} Re}{\tilde{Q}} \right) \right)^2},$$

$$\frac{Re}{\tilde{f}} \left(\frac{\partial \tilde{f}}{\partial Re} \right)_{\tilde{Q}, \phi} = \frac{-1}{\ln \left(\frac{1}{3.7} \frac{\pi}{4} \frac{\tilde{\varepsilon} Re}{\tilde{Q}} \right)}, \quad \frac{\phi}{\tilde{f}} \left(\frac{\partial \tilde{f}}{\partial \phi} \right)_{\tilde{Q}, Re} = 0,$$

$$\frac{\tilde{Q}}{\tilde{f}} \left(\frac{\partial \tilde{f}}{\partial \tilde{Q}} \right)_{\phi, Re} = \frac{1}{\ln \left(\frac{1}{3.7} \frac{\pi}{4} \frac{\tilde{\varepsilon} Re}{\tilde{Q}} \right)}. \tag{D13}$$

D.2.2 *Turbulence, smooth channel*

For a smooth-wall channel ($\varepsilon \to 0$), the Colebrook–White equation (Colebrook 1939) reduces to

$$\tilde{f} = \left\{ -2.0 \log_{10} \left(\frac{2.51}{Re \sqrt{\tilde{f}}} \right) \right\}^{-2}. \tag{D14}$$

Differentiation provides the needed differentials in (D3)

$$\frac{\tilde{f}}{\tilde{B}} \left(\frac{\partial \tilde{B}}{\partial \tilde{f}} \right)_{\tilde{Q}, \phi, Re} = 1 + \frac{\tilde{f}}{\tilde{B}} \left[\frac{1}{\left[\ln \left(\frac{2.51}{\sqrt{\tilde{f}} Re} \right) - 1 \right]^2} \right],$$

$$\frac{Re}{\tilde{B}}\left(\frac{\partial \tilde{B}}{\partial Re}\right)_{\tilde{f},\tilde{Q},\phi} = \frac{\tilde{f}}{\tilde{B}}\left[\frac{2}{\left[\ln\left(\frac{2.51}{\sqrt{\tilde{f}}Re}\right)-1\right]^2}\right], \qquad \frac{\phi}{\tilde{B}}\left(\frac{\partial \tilde{B}}{\partial \phi}\right)_{\tilde{f},\tilde{Q},Re} = 0,$$

$$\frac{\tilde{Q}}{\tilde{B}}\left(\frac{\partial \tilde{B}}{\partial \tilde{Q}}\right)_{\tilde{f},\phi,Re} = 0, \quad \frac{Re}{\tilde{f}}\left(\frac{\partial \tilde{f}}{\partial Re}\right)_{\tilde{Q},\phi} = \frac{2}{\ln\left(\frac{2.51}{\sqrt{\tilde{f}}Re}\right)-1},$$

$$\frac{\phi}{\tilde{f}}\left(\frac{\partial \tilde{f}}{\partial \phi}\right)_{\tilde{Q},Re} = 0, \quad \frac{\tilde{Q}}{\tilde{f}}\left(\frac{\partial \tilde{f}}{\partial \tilde{Q}}\right)_{\phi,Re} = 0.$$

$$(D15)$$

D.2.3 *Low-Reynolds-number turbulence, smooth channel*

For certain Reynolds-number regimes of flow in a smooth channel ($\varepsilon \to 0$), approximations for the friction factor have been formulated, such as Blasius' formula and empirical relations. These are often in the following form (Uylings 1977):

$$\tilde{f} = \frac{c_1}{Re^{c_2}}. \tag{D16}$$

Differentiation provides the needed differentials in (D3)

$$\frac{\tilde{f}}{\tilde{B}}\left(\frac{\partial \tilde{B}}{\partial \tilde{f}}\right)_{\tilde{Q},\phi,Re} = 1, \qquad \frac{Re}{\tilde{B}}\left(\frac{\partial \tilde{B}}{\partial Re}\right)_{\tilde{f},\tilde{Q},\phi} = 0, \qquad \frac{\phi}{\tilde{B}}\left(\frac{\partial \tilde{B}}{\partial \phi}\right)_{\tilde{f},\tilde{Q},Re} = 0,$$

$$\frac{\tilde{Q}}{\tilde{B}}\left(\frac{\partial \tilde{B}}{\partial \tilde{Q}}\right)_{\tilde{f},\phi,Re} = 0, \qquad \frac{Re}{\tilde{f}}\left(\frac{\partial \tilde{f}}{\partial Re}\right)_{\tilde{Q},\phi} = -c_2, \qquad \frac{\phi}{\tilde{f}}\left(\frac{\partial \tilde{f}}{\partial \phi}\right)_{\tilde{Q},Re} = 0,$$

$$\frac{\tilde{Q}}{\tilde{f}}\left(\frac{\partial \tilde{f}}{\partial \tilde{Q}}\right)_{\phi,Re} = 0.$$

$$(D17)$$

Substituting everything into (D3) results in $(Re/\tilde{Q})\,\partial \tilde{Q}/\partial Re = (7-c_2)/4$, resulting in $x = (7-c_2)/(3-c_2)$. For Blasius' equation (B12), x reduces to $x = 27/11$ and for the empirical relation (B14) x reduces to $x = 17/7$.

D.3 *Turbulent flow of non-Newtonian fluids, smooth channel*

D.3.1 *Power-law fluid*

Turbulent pipe flow of non-Newtonian power-law fluids at low Reynolds numbers in a smooth circular channel ($\varepsilon \to 0$) described by Dodge and Metzner (Dodge & Metzner 1959) is given in the following implicit relation for the Darcy friction factor f:
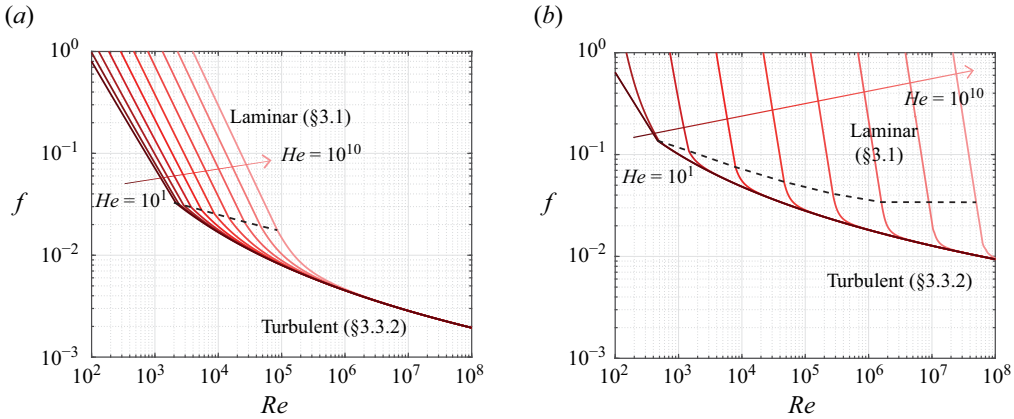
Figure 7. Friction factor as function of the Reynolds number for Herschel–Bulkley fluids. The dashed black line indicates the transition from laminar to turbulent flow. The red-scale lines represent constant values of the Hedström number from $10^1, 10^2, \ldots, 10^{10}$ with decreasing brightness. Panels show (*a*) $n = 0.5$ and (*b*) $n = 1.5$.

$$\frac{2}{\sqrt{f}} = \frac{4}{n^{0.75}} \log_{10}\left(Re\left(\frac{f}{4}\right)^{1-n/2} \right) - \frac{0.4}{n^{1.2}}. \tag{D18}$$

Differentiation provides the needed differentials in (D3)

$$\frac{\tilde{f}}{\tilde{B}}\left(\frac{\partial \tilde{B}}{\partial \tilde{f}}\right)_{\tilde{Q},\phi,Re} = 1 - \frac{\tilde{f}}{\tilde{B}}(4-3n)\left(\frac{n^{0.75}\ln(10)}{4\sqrt{\tilde{f}}} + 1 - \frac{n}{2}\right)^{-2}\frac{n^{0.75}\ln(10)}{8\sqrt{\tilde{f}}},$$

$$\frac{Re}{\tilde{B}}\left(\frac{\partial \tilde{B}}{\partial Re}\right)_{\tilde{f},\tilde{Q},\phi} = 0, \qquad \frac{\phi}{\tilde{B}}\left(\frac{\partial \tilde{B}}{\partial \phi}\right)_{\tilde{f},\tilde{Q},Re} = 0, \qquad \frac{\tilde{Q}}{\tilde{B}}\left(\frac{\partial \tilde{B}}{\partial \tilde{Q}}\right)_{\tilde{f},\phi,Re} = 0,$$

$$\frac{Re}{\tilde{f}}\left(\frac{\partial \tilde{f}}{\partial Re}\right)_{\tilde{Q},\phi} = -\left(\frac{n^{0.75}\ln(10)}{4\sqrt{\tilde{f}}} + 1 - \frac{n}{2}\right)^{-1},$$

$$\frac{\phi}{\tilde{f}}\left(\frac{\partial \tilde{f}}{\partial \phi}\right)_{\tilde{Q},Re} = 0, \qquad \frac{\tilde{Q}}{\tilde{f}}\left(\frac{\partial \tilde{f}}{\partial \tilde{Q}}\right)_{\phi,Re} = 0. \tag{D19}$$

D.3.2 *Herschel–Bulkley fluid*

For a turbulent flow of a Herschel–Bulkley fluid in a smooth circular channel ($\varepsilon \to 0$), Torrance (Garcia & Steffe 1986) developed a relationship for the Darcy friction factor

$$\frac{2}{\sqrt{\tilde{f}}} = 0.45 - \frac{2.75}{n} + \frac{1.97}{n}\ln(1-\phi) + \frac{1.97}{n}\ln\left(Re\left(\frac{3n+1}{4n}\right)^n\left(\frac{\tilde{f}}{4}\right)^{1-\frac{n}{2}} \right). \tag{D20}$$

Differentiation provides the needed differentials in (D3)

$$\frac{\tilde{f}}{\tilde{B}}\left(\frac{\partial \tilde{B}}{\partial \tilde{f}}\right)_{\tilde{Q},\phi,Re} = 1 - \frac{\tilde{f}}{\tilde{B}}\frac{4 - 3n + \frac{4\phi}{1-\phi}}{\left(\frac{n}{1.97\sqrt{\tilde{f}}} + \frac{\phi}{1-\phi} + 1 - \frac{n}{2}\right)}\frac{\frac{1}{2}n}{1.97\sqrt{\tilde{f}}},$$

$$\frac{Re}{\tilde{B}}\left(\frac{\partial \tilde{B}}{\partial Re}\right)_{\tilde{f},\tilde{Q},\phi} = 0, \qquad \frac{\phi}{\tilde{B}}\left(\frac{\partial \tilde{B}}{\partial \phi}\right)_{\tilde{f},\tilde{Q},Re} = -\frac{\tilde{f}}{\tilde{B}}\frac{\left(\frac{4n}{1.97\sqrt{\tilde{f}}} + n\right)\frac{\phi}{(1-\phi)^2}}{\left(\frac{n}{1.97\sqrt{\tilde{f}}} + \frac{\phi}{1-\phi} + 1 - \frac{n}{2}\right)^2},$$

$$\frac{\tilde{Q}}{\tilde{B}}\left(\frac{\partial \tilde{B}}{\partial \tilde{Q}}\right)_{\tilde{f},\phi,Re} = 0, \qquad \frac{Re}{\tilde{f}}\left(\frac{\partial \tilde{f}}{\partial Re}\right)_{\tilde{Q},\phi} = \frac{-1}{\frac{n}{1.97\sqrt{\tilde{f}}} + 1 - \frac{n}{2}},$$

$$\frac{\phi}{\tilde{f}}\left(\frac{\partial \tilde{f}}{\partial \phi}\right)_{\tilde{Q},Re} = \frac{\frac{\phi}{1-\phi}}{\frac{n}{1.97\sqrt{\tilde{f}}} + 1 - \frac{n}{2}}, \qquad \frac{\tilde{Q}}{\tilde{f}}\left(\frac{\partial \tilde{f}}{\partial \tilde{Q}}\right)_{\phi,Re} = 0.$$

$$(D21)$$

Appendix E. Extra figures for Herschel–Bulkley fluids ($n = 0.5$ and $n = 1.5$)

For a Herschel–Bulkley fluid, the graphs for the friction factor as function of the Reynolds number and the optimisation graphs have to be made for every value of n separately. For readability, in the main text, it is chosen to limit to $n = 1$, and therefore, the graphs for other values of n are given in this section. Figure 7 shows the friction factor f as function of the Reynolds number Re for both laminar and turbulent flow. The optimisation graphs for laminar flow of a Herschel–Bulkley fluid for $n = 0.5$, $n = 1.0$ and $n = 1.5$ and covering all n are given in figure 8. The optimisation graphs for turbulent flow for $n = 0.5$ and $n = 1.5$ are given in figure 9. Finally, figure 10 shows x as function of Re for $n = 0.5$ and $n = 1.5$.

Appendix F. Example of network optimisation

In this section, an example illustrates how the optimisation theory could be applied. Imagine a water distribution system, which aims to distribute water from a main channel to 8 endpoints. The requested output at each endpoint is 12.5 l min^{-1}, which means that the main channel should supply $Q_0 = 100$ l min^{-1}. The begin node is at (0,0) and the end nodes are chosen to be placed equidistantly along an arc with a radius of curvature of 4 m (see figure 11a). It is chosen to have symmetric bifurcations, with 4 levels of branchings, denoted by indices 0 to 3. The channels are drawn tubes with a wall roughness of $\varepsilon = 0.0025$ mm, and water is a Newtonian fluid ($n = 1$, $\tau_0 = 0$) with viscosity $\mu' = 1$ mPa s and fluid density $\rho = 1000$ kg m^{-3}.

The design procedure as described in § 5 is followed. In step (i), the cost factor could be chosen or derived from a constraint (see also Smink *et al.* 2023). Here, for the optimisation is chosen to base the cost factor on a constraint for the outlet channel size. The radius of the outlet channels is chosen to be $R_3 = 7.5$ mm, a common channel size for tap water. The cost factor can be retrieved in the following manner. The Reynolds number of the flow in the outlet channels is set by the constraint to be $Re_3 = 1.768 \times 10^4$. This means that we have a turbulent flow of a Newtonian fluid in rough-wall channels in the network. From
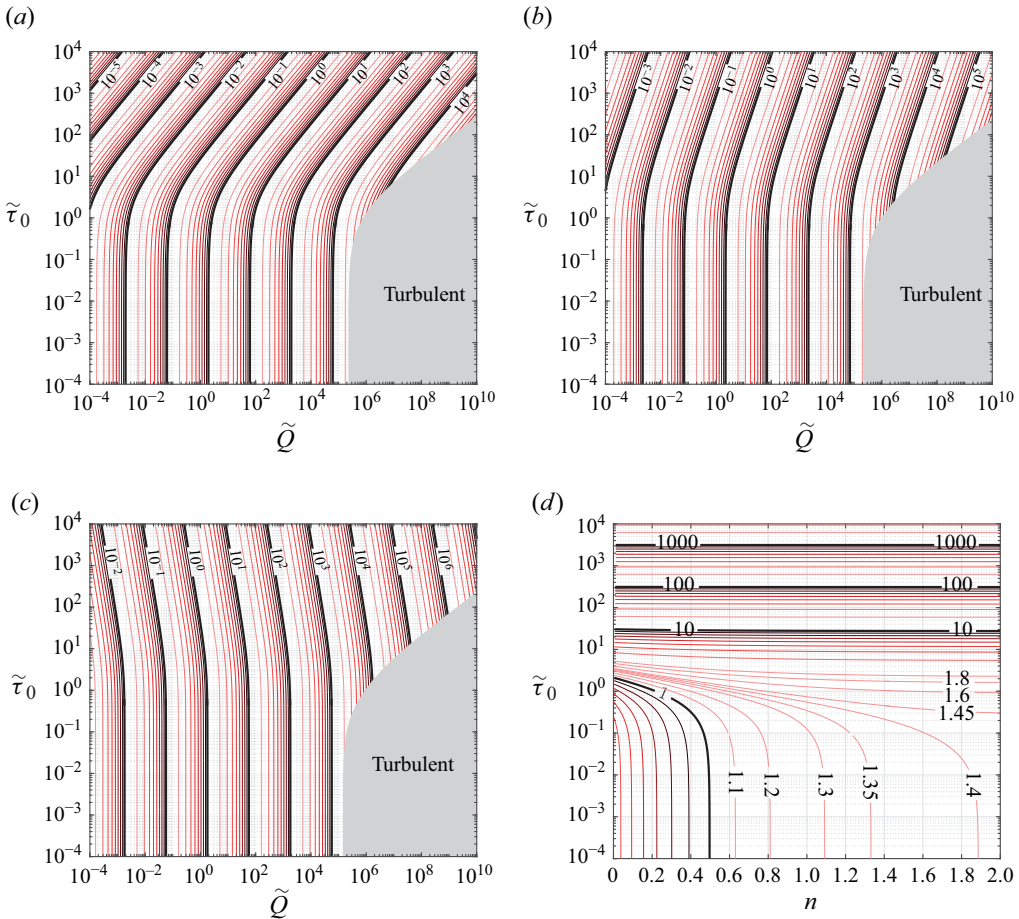
Figure 8. Contour plots of the optimisation condition for a laminar flow of a Herschel–Bulkley fluid (3.8). The red-scale contour lines represent values $2 \times 10^x, 3 \times 10^x, \ldots 9 \times 10^x$ with decreasing brightness. (*a*) Optimal Reynolds number as a function of $\tilde{\tau}_0$ and $\tilde{Q}$ for a Herschel–Bulkley fluid with $n = 0.5$. (*b*) Optimal Reynolds number as a function of $\tilde{\tau}_0$ and $\tilde{Q}$ for a Herschel–Bulkley fluid with $n = 1.0$. (*c*) Optimal Reynolds number as a function of $\tilde{\tau}_0$ and $\tilde{Q}$ for a Herschel–Bulkley fluid with $n = 1.5$. (*d*) Optimal $\tilde{R}^3/\tilde{Q}$ as function of n and $\tilde{\tau}_0$. This optimisation plot covers all laminar flows of Herschel–Bulkley fluids.

the given parameters, it is known that $\tilde{Q}\alpha^{-1/4} = \rho^{3/2}\mu'^{-7/4}Q = 1.17 \times 10^6$ m$^{3/4}$ W$^{-1/4}$ and $\tilde{\varepsilon}\alpha^{-1/4} = \rho^{1/2}\mu'^{-3/4}\varepsilon = 0.0141$ m$^{3/4}$ W$^{-1/4}$. We will use the graphical approach to avoid tedious calculations. Figure 3(*a*) shows the corresponding optimisation graph, using which the combination of Re, $\tilde{Q}\alpha^{-1/4}$ and $\tilde{\varepsilon}\alpha^{-1/4}$ gives the corresponding $\tilde{Q}$, $\tilde{\varepsilon}$ and α. This graph shows that the given combination shows that $\tilde{Q}_3 \approx 9.0 \times 10^6$, $\tilde{\varepsilon} \approx 0.11$ and $\alpha \approx 3.5 \times 10^3$ W m^{-3}. The dimensionless flow rates in the other three levels are then $\tilde{Q}_2 \approx 1.8 \times 10^7$, $\tilde{Q}_1 \approx 3.6 \times 10^7$ and $\tilde{Q}_0 \approx 7.2 \times 10^7$.

In step (ii), the optimal radius for one channel is determined. In this case, the channel radius and Reynolds number for the outlet channels (level 3) are already known because of the given constraint. Step (iii) is then carried out for obtaining the other optimal channel radii R_i via the optimal Reynolds numbers in the channels, by repeating step (ii) for each channel. Using $\tilde{\varepsilon}$ and the determined $\tilde{Q}_i$ ($i = 0, 1, 2, 3$), the other optimal values of Re_i are obtained from figure 3(*a*). These are $Re_2 \approx 2.6 \times 10^4$, $Re_1 \approx 4.0 \times 10^4$ and $Re_0 \approx$
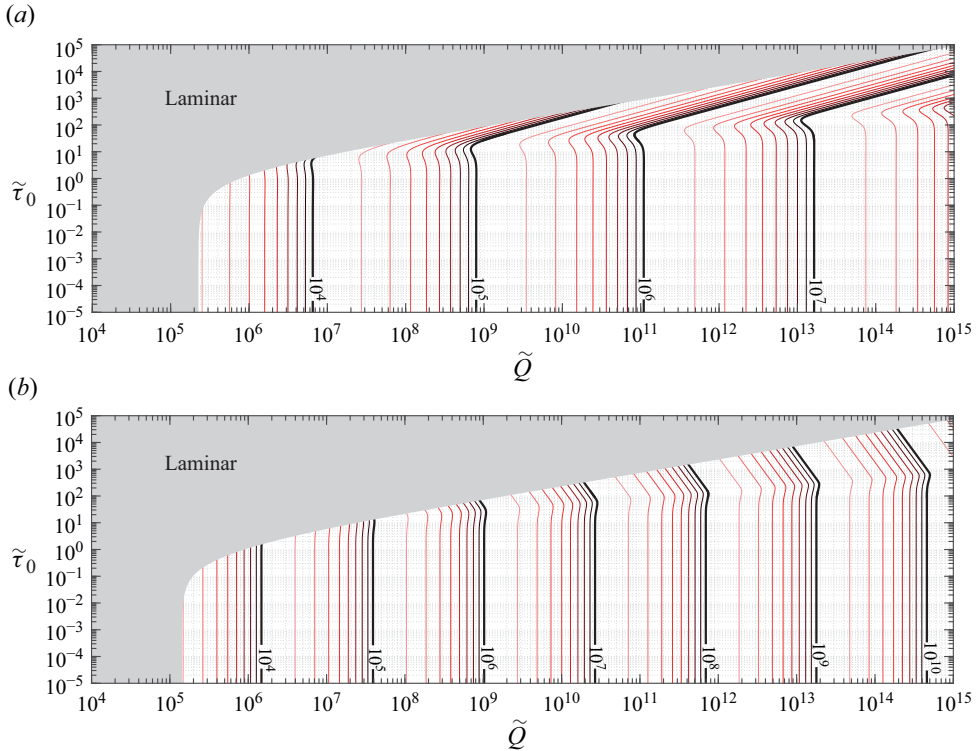
(*a*)

(*b*)

Figure 9. Contour plots of the optimal Reynolds number as a function of $\tilde{Q}$ and $\tilde{\tau}_0$ for a turbulent flow of a Herschel–Bulkley fluid (3.17) at constant n. The red-scale contour lines represent the Reynolds numbers $2 \times 10^x, 3 \times 10^x, \ldots 9 \times 10^x$ with decreasing brightness. Panels show (*a*) $n = 0.5$ and (*b*) $n = 1.5$.

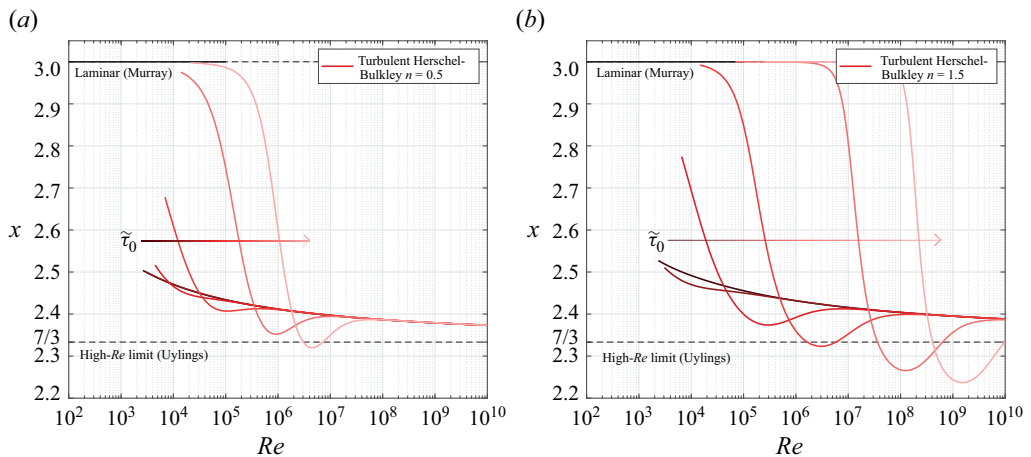(*a*)   (*b*)

Figure 10. Plot of x (4.1) as function of Re for turbulent flow of a Herschel–Bulkley fluid (Torrance) as discussed in § 3.3.2. The dashed lines for $x = 3$ and $x = 7/3$ show the expected limit cases for laminar flow and high-turbulent flow, respectively (Uylings 1977). The different lines are for $\tilde{\tau}_0 \in [0.1, 0.25, 1, 2.5, 10, 25]$. Panels show (*a*) $n = 0.5$ and (*b*) $n = 1.5$.
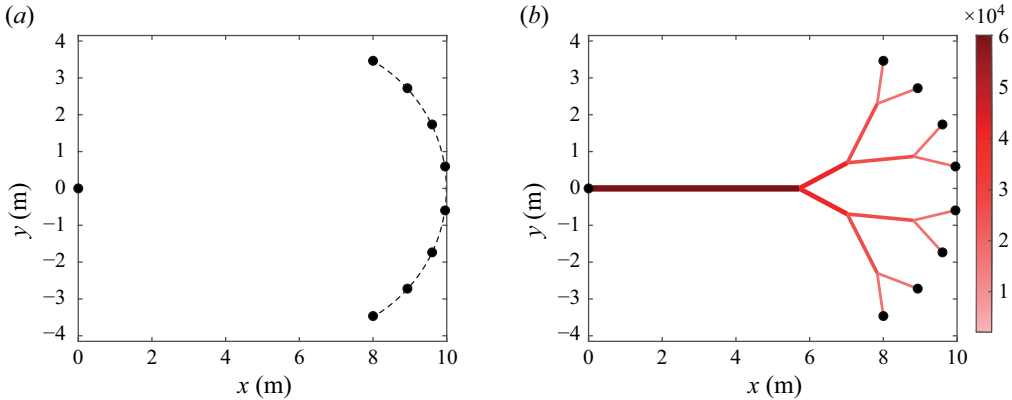
Figure 11. Example of optimisation of a branched fluidic network for a water distribution network. (*a*) The position coordinates of the begin point and the endpoints are given and represented by black circles, where the endpoints are located equidistantly along an arc with a radius of curvature of 4 m. (*b*) The obtained optimised water distribution network. The colour indicates the Reynolds number of the flow within the channel. For visibility, the channel diameters are magnified in the plot.

6.0×10^4. From here, the channel radii are calculated using the definition of the Reynolds number (2.4): $R_2 \approx 10.2$ mm, $R_1 \approx 13.3$ mm, $R_0 \approx 17.7$ mm. These are the optimised channel radii. Finally, the positions of the branching point locations are calculated in step (iv) (see Appendix A.1), resulting in the full geometry of the optimised water distribution network, presented in figure 11(*b*). In each level, the lengths of the channels are the same ($L_0 \approx 5.71$, $L_1 \approx 1.48$, $L_2 \approx 1.80$ and $L_3 \approx 1.18$ m), and therefore the same holds for the pressure drop in the channels in each level ($\Delta p_0 \approx 4.85$, $\Delta p_1 \approx 1.42$, $\Delta p_2 \approx 1.97$ and $\Delta p_3 \approx 1.47$ kPa).

REFERENCES

General requirements for water supply installations, Tech. Rep. NEN 1006+A1. Koninklijk Nederlands Normalisatie-instituut.
BEJAN, A. 2013 Turbulent duct flow, chap.8. pp. 369–397. John Wiley & Sons, Ltd..
BEJAN, A. & LORENTE, S. 2013 Constructal law of design and evolution: physics, biology technology, and society. *J. Appl. Phys.* **113** (15), 151301.
BEJAN, A., ROCHA L.A., O. & LORENTE, S. 2000 Thermodynamic optimization of geometry: T- and Y-shaped constructs of fluid streams. *Intl J. Therm. Sci.* **39** (9), 949–960.
BERGER, S.A. & JOU, L.-D. 2000 Flows in stenotic vessels. *Annu. Rev. Fluid Mech.* **32** (2000), 347–382.
BLASIUS, H. 1912 Das Aehnlichkeitsgesetz bei Reibungsvorgangen. *Zeitschrift des Vereines deutscher Ingenieure* **639**, 1–5.
BLASIUS, H. 1913 Das Aehnlichkeitsgesetz bei reibungsvorgangen in flüssigkeiten. *Mitteilungen über Forschungsarbeiten Auf Dem Gebiete Des Ingenieurwesens* **131**, 1–41.
BURTON, H.E. & ESPINO, D.M. 2019 The effect of mechanical overloading on surface roughness of the coronary arteries. *Appl. Bionics Biomech.* **1**, 2784172.
CALMET, H., GAMBARUTO, A.M., BATES, A.J., VÁZQUEZ, M., HOUZEAUX, C. & DOORLY, D.J. 2016 Large-scale CFD simulations of the transitional and turbulent regime for the large human airways during rapid inhalation. *Comput. Biol. Med.* **69**, 166–180.
CHILTON, R.A. & STAINSBY, R. 1998 Pressure loss equations for laminar and turbulent non-newtonian pipe flow. *J. Hydraul. Engng* **124** (5), 522–529.
COLEBROOK, C.F. 1939 Turbulent flow in pipes, with particular reference to the transition region between the smooth and rough pipe laws. *J. Inst. Civil Engrs* **11** (4), 133–156.
DARBY, R., MUN, R. & BOGER, D.V. 1992 Predict friction loss in slurry pipes. *Adv. Engng* **99**, 116–119.
VAN DEVENTER, H., HOUBEN, R. & KOLDEWEIJ, R. 2013 New atomization nozzle for spray drying. *Dry. Technol.* **31** (8), 891–897.
DI CARLO, D. 2009 Inertial microfluidics. *Lab Chip* **9** (21), 3038–3046.

DODGE, D.W. & METZNER, A.B. 1959 Turbulent flow of non-newtonian systems. *AIChE J.* **5** (2), 189–204.

DONG, Z., WEN, Z., ZHAO, F., KUHN, S. & NOËL, T. 2021 Scale-up of micro- and milli-reactors: an overview of strategies, design principles and applications. *Chem. Engng Sci. X* **10**, 100097.

EMERSON, D.R. & BARBER, R.W. 2012 A Design Approach for Non-Newtonian Power-Law Flow in Rectangular Micro-channels Based on Murray's Law, In *Proceedings of the 3rd European Conference on Microfluidics*.

EMERSON, D.R., CIEŚLICKI, K., GU, X. & BARBER, R.W. 2006 Biomimetic design of microfluidic manifolds based on a generalised Murray's law. *Lab Chip* **6** (3), 447–454.

EVERTS, M., ROBBERTSE, P. & SPITHOLT, B. 2022 The effects of surface roughness on fully developed laminar and transitional flow friction factors and heat transfer coefficients in horizontal circular tubes. *Intl J. Heat Mass Transfer* **189**, 122724.

FORGACS, O.L., ROBERTSON, A.A. & MASON, S.G. 1957 The hydrodynamic behaviour of papermaking fibres. In *Fundamentals of papermaking fibres—1st fundamental research symposium*, vol. 1, pp. 447–473.

GARCIA, E.J. & STEFFE, J.F. 1986 Comparison of friction factor equations for non-Newtonian fluids in pipe flow. *J. Food Process Engng* **9** (2), 93–120.

GROSSMAN, J. & CARPENTER, W.L. 1968 A study of pipeline flow characteristics of pulp and papermill sludges. Tech. Rep. 213.National council of the paper industry for air and stream improvement.

GUMPERT, B., WIELAND, C. & SPLIETHOFF, H. 2019 Thermo-hydraulic simulation of district heating systems. *Geothermics* **82**, 244–253.

HA, H., KVITTING, J.P., DYVERFELDT, P. & EBBERS, T. 2019 Validation of pressure drop assessment using 4D flow MRI-based turbulence production in various shapes of aortic stenoses. *Magn. Reson. Med.* **81** (2), 893–906.

HA, H., ZIEGLER, M., WELANDER, M., BJARNEGÅRD, N., CARLHÄLL, C.-J., LINDENBERGER, M., LÄNNE, T., EBBERS, T. & DYVERFELDT, P. 2018 Age-related vascular changes affect turbulence in aortic blood flow. *Frontiers Physiol.* **9**, 36.

HAALAND, S.E. 1983 Simple and explicit formulas for the friction factor in turbulent pipe flow. *ASME J. Fluids Engng* **105** (1), 89–90.

HANKS, R.W. & RICKS, B.L. 1974 Laminar-turbulent transition in flow of pseudoplastic fluids with yield stresses. *J. Hydronaut.* **8** (4), 163–166.

HERSCHEL, W.H. & BULKLEY, R. 1926 Konsistenzmessungen von Gummi-Benzollösungen. *Kolloid-Zeitschrift* **39** (4), 291–300.

HOOPER, G. 1977 Diameters of bronchi at asymmetrical divisions. *Respir. Physiol.* **31** (3), 291–294.

HUTCHINS, G.M., MINER, M.M. & BOITNOTT, J.K. 1976 Vessel caliber and branch-angle of human coronary artery branch-points. *Circulat. Res* **38** (6), 572–576.

KAMIS, Y.E., PRAKASH, S., BREUGEM, W.-P. & ERAL, H.B. 2023 Controlling the breakup of spiralling jets: results from experiments, nonlinear simulations and linear stability analysis. *J. Fluid Mech.* **956**, A24.

KAMIYA, A., TOGAWA, T. & YAMAMOTA, A. 1974 Theoretical relationship between the optimal models of the vascular tree. *Bull. Math. Biol.* **36**, 311–323.

KASSAB, G.S., RIDER, C.A., TANG, N.J. & FUNG, Y.-C.B. 1993 Morphometry of pig coronary arterial trees. *Am. J. Physiolo. - Heart Circulat. Physiol.* **265** (1), H350–H365.

KELCH, I.D., BOGLE, G., SANDS, G.B., PHILLIPS, A.R.J., LEGRICE, I.J. & ROD DUNBAR, P. 2015 Organ-wide 3D-imaging and topological analysis of the continuous microvascular network in a murine lymph node. *Sci. Rep-UK.* **5** (1), 16534.

KOU, J., CHEN, Y., ZHOU, X., LU, H., WU, F. & FAN, J. 2014 Optimal structure of tree-like branching networks for fluid flow. *Physica A* **393**, 527–534.

KU, D.N. 1997 Blood flow in arteries. *Annu. Rev. Fluid Mech.* **29** (1), 399–434.

LIU, Y., LI, J. & SMITS, A.J. 2019 Roughness effects in laminar channel flow. *J. Fluid Mech.* **876**, 1129–1145.

LU, X., LIU, C., HU, G. & XUAN, X. 2017 Particle manipulations in non-Newtonian microfluidics: a review. *J. Colloid Interface Sci.* **500**, 182–201.

LUNDELL, F., SÖDERBERG, L.D. & ALFREDSSON, P.H. 2011 Fluid mechanics of papermaking. *Annu. Rev. Fluid Mech.* **43** (1), 195–217.

MACDONALD, M.J., CHU, C.-F., GUILLOIT, P.P. & NG, K.M. 1991 A generalized Blake-Kozeny equation for multisized spherical particles. *AIChE J.* **37** (10), 1583–1588.

MAYROVITZ, H.N. 1987 An optimal flow-radius equation for microvessel non-Newtonian blood flow. *Microvasc. Res.* **34** (3), 380–384.

MIGUEL, A.F. 2018 A general model for optimal branching of fluidic networks. *Physics A* **512**, 665–674.

MIGUEL, A.F. & ROCHA, L.A.O. 2018 *Tree-Shaped Fluid Flow and Heat Transfer*. 1st edn. Springer. iSBN 978-3-319-73259-6.

MOLLER, K. 1976 A correlation of pipe friction data for paper pulp suspensions. *Ind. Engng Chem. Proc. Design Develop.* **15** (1), 16–19.

MOODY, L.F. 1944 Friction factors for pipe flow. *Trans. ASME* **66** (8), 671–684.

MORINI, G.L. & SPIGA, M. 1998 Slip flow in rectangular microtubes. *Microscale Therm. Engng* **2** (4), 273–282.

MORRIS, P.D. *et al.* 2016 Computational fluid dynamics modelling in cardiovascular medicine. *Heart* **102** (1), 18–28.

MURRAY, C.D. 1926*a* The physiological principle of minimum work applied to the angle of branching of arteries. *J. Gen. Physiol.* **9** (6), 835–841.

MURRAY, C.D. 1926*b* The physiological principle of minimum work. I. The vascular system and the cost of blood volume. *Proc. Natl. Acad. Sci.* **12** (3), 207–214.

OKA, S. & NAKAI, M. 1987 Optimality principle in vascular bifurcation. *Biorheology* **24** (6), 737–751.

OLSON, D.E., DART, G.A. & FILLEY, G.F. 1970 Pressure drop and fluid flow regime of air inspired into the human lung. *J. Appl. Physiol.* **28** (4), 482–494.

PONALAGUSAMY, R. 2012 Mathematical analysis on effect of non-Newtonian behavior of blood on optimal geometry of microvascular bifurcation system. *J. Frankl. Inst.* **349** (9), 2861–2874.

REICHOLD, J., STAMPANONI, M., KELLER, A.L., BUCK, A., JENNY, P. & WEBER, B. 2009 Vascular graph model to simulate the cerebral blood flow in realistic vascular networks. *J. Cerebral Blood Flow & Metabolism* **29** (8), 1429–1443.

REINER, M. 1926 Ueber die Strömung einer elastischen Flüssigkeit durch eine Kapillare. *Kolloid-Zeitschrift* **39** (1), 80–87.

REVELLIN, R., ROUSSET, F., BAUD, D. & BONJOUR, J. 2009 Extension of Murray's law using a non-Newtonian model of blood flow. *Theor. Biol. Med. Model.* **6** (1), 7.

ROSSITTI, S. & LÖFGREN, J. 1993 Vascular dimensions of the cerebral arteries follow the principle of minimum work. *Stroke* **24** (3), 371–377.

VAN DER SCHANS, M.L., BRUSSEE, L., NIEKUS, P. & LEUNK, I. 2015 Energieverbruik drinkwaterwinning. Tech. Rep. 039.KWR Watercycle Research Institute.

SEXTON, Z.A., HUDSON, A.R., HERRMANN, J.E., SHIWARSKI, D.J., PHAM, J., SZAFRON, J.M., WU, S.M., SKYLAR-SCOTT, M., FEINBERG, A.W. & MARSDEN, A. 2023 Rapid model-guided design of organ-scale synthetic vasculature for biomanufacturing. arXiv: 2308.07586.

SHAQFEH, E., LIPKOWITZ, G., KISHNA, N., COATES, I. & DESIMONE, J. 2023 Bioinspired fluidic design for additive manufacturing.

SHERMAN, T.F. 1981 On connecting large vessels to small: the meaning of Murray's law. *J. Gen. Physiol.* **78** (4), 431–453.

SIDDIQUI, O.K. & ZUBAIR, S.M. 2017 Efficient energy utilization through proper design of microchannel heat exchanger manifolds: a comprehensive review. *Renew. Sustainable Energy Rev.* **74**, 969–1002.

SINGHAL, S., HENDERSON, R. & HORSFIELD, K. 1973 Morphometry of the human pulmonary arterial tree. *Circulat. Res.* **33** (2), 190–197.

SKYLAR-SCOTT, M.A., MUELLER, J., VISSER, C.W. & LEWIS, J.A. 2019 Voxelated soft matter via multimaterial multinozzle 3D printing. *Nature* **575** (7782), 330–335.

SMINK, J.S., VENNER, C.H., VISSER, C.W. & HAGMEIJER, R. 2023 Engineering of branched fluidic networks that minimise energy dissipation. *J. Fluid Mech.* **967**, A6.

STEIN, P.D. & SABBAH, H.N. 1976 Turbulent blood flow in the ascending aorta of humans with normal and diseased aortic valves. *Circulat. Res.* **39** (1), 58–65.

STEINEGGER, J., WALLNER, S., GREIML, M. & KIENBERGER, T. 2023 A new quasi-dynamic load flow calculation for district heating networks. *Energy* **266**, 126410.

STEPHENSON, D. & LOCKERBY, D.A. 2016 A generalized optimization principle for asymmetric branching in fluidic networks. *Proc. R. Soc. A* **472** (2191), 20160451.

STEPHENSON, D., PATRONIS, A., HOLLAND, D.M. & LOCKERBY, D.A. 2015 Generalizing Murray's law: an optimization principle for fluidic networks of arbitrary shape and scale. *J. Appl. Phys.* **118** (17), 174302.

SWAMEE, P.K. & AGGARWAL, N. 2011 Explicit equations for laminar flow of Herschel–Bulkley fluids. *Canadian J. Chem. Engng* **89** (6), 1426–1433.

SZNITMAN, J. 2022 Revisiting airflow and aerosol transport phenomena in the deep lungs with microfluidics. *Chem. Rev.* **122** (7), 7182–7204.

TESCH, K. 2010 On some extensions of Murray's law. *Task Q.* **14**, 227–235.

TOWLER, G.P. & SINNOTT, R.K. 2013 *Chemical Engineering Design*. 2nd edn. Butterworth-Heinemann. ISBN 978-0-08-096659-5

UYLINGS, H.B.M. 1977 Optimization of diameters and bifurcation angles in lung and vascular tree structures. *Bull. Math. Biol.* **39** (5), 509–520.

VISSER, C.W., AMATO, D.N., MUELLER, J. & LEWIS, J.A. 2019 Architected polymer foams via direct bubble writing. *Adv. Mater.* **31** (46), 1904668.

VISSER, C.W., KAMPERMAN, T., KARBAAT, L.P., LOHSE, D. & KARPERIEN, M. 2018 In-air microfluidics enables rapid fabrication of emulsions, suspensions, and 3D modular (bio)materials. *Sci. Adv.* **4** (1), eaao1175.

WANG, G.R., YANG, F. & ZHAO, W. 2014 There can be turbulence in microfluidics at low Reynolds number. *Lab Chip* **14** (8), 1452–1458.

WEISBACH, J.L. 1845 *Lehrbuch der Ingenieur- Und Maschinen-Mechanik. Erster Theil: Theoretische Mechanik*. 1st edn. Friedrich Vieweg und Sohn.

WHITESIDES, G. 2006 The origins and the future of microfluidics. *Nature* **442** (7101), 368–373.

WILLIAMS, H.R., TRASK, R.S., WEAVER, P.M. & BOND, I.P. 2008 Minimum mass vascular networks in multifunctional materials. *J. R. Soc. Interface* **5** (18), 55–65.

WOLDENBERG, M.J. & HORSFIELD, K. 1986 Relation of branching angles to Optimality for four cost principles. *J. Theor. Biol.* **122** (2), 187–204.

XU, P., SASMITO, A.P., YU, B. & MUJUMDAR, A.S. 2016 Transport phenomena and properties in treelike networks. *Appl. Mech. Rev.* **68** (4), 040802.

ZAMIR, M. 1977 Shear forces and blood vessel radii in the cardiovascular system. *J. Gen. Physiol.* **69** (4), 449–461.

ZHANG, J., YAN, S., YUAN, D., ALICI, G., NGUYEN, N.-T., WARKIANI, M.E. & LI, W. 2016 Fundamentals and applications of inertial microfluidics: a review. *Lab Chip* **16** (1), 10–34.

ZHENG, X., SHEN, G., WANG, C., LI, Y., DUNPHY, D., HASAN, T., BRINKER, C.J. & SU, B.L. 2017 Bio-inspired Murray materials for mass transfer and activity. *Nat. Commun.* **8** (1), 14921.

ZHOU, B. *et al.* 2024 Universal Murray's law for optimised fluid transport in synthetic structures. *Nat. Commun.* **15** (1), 3652.